

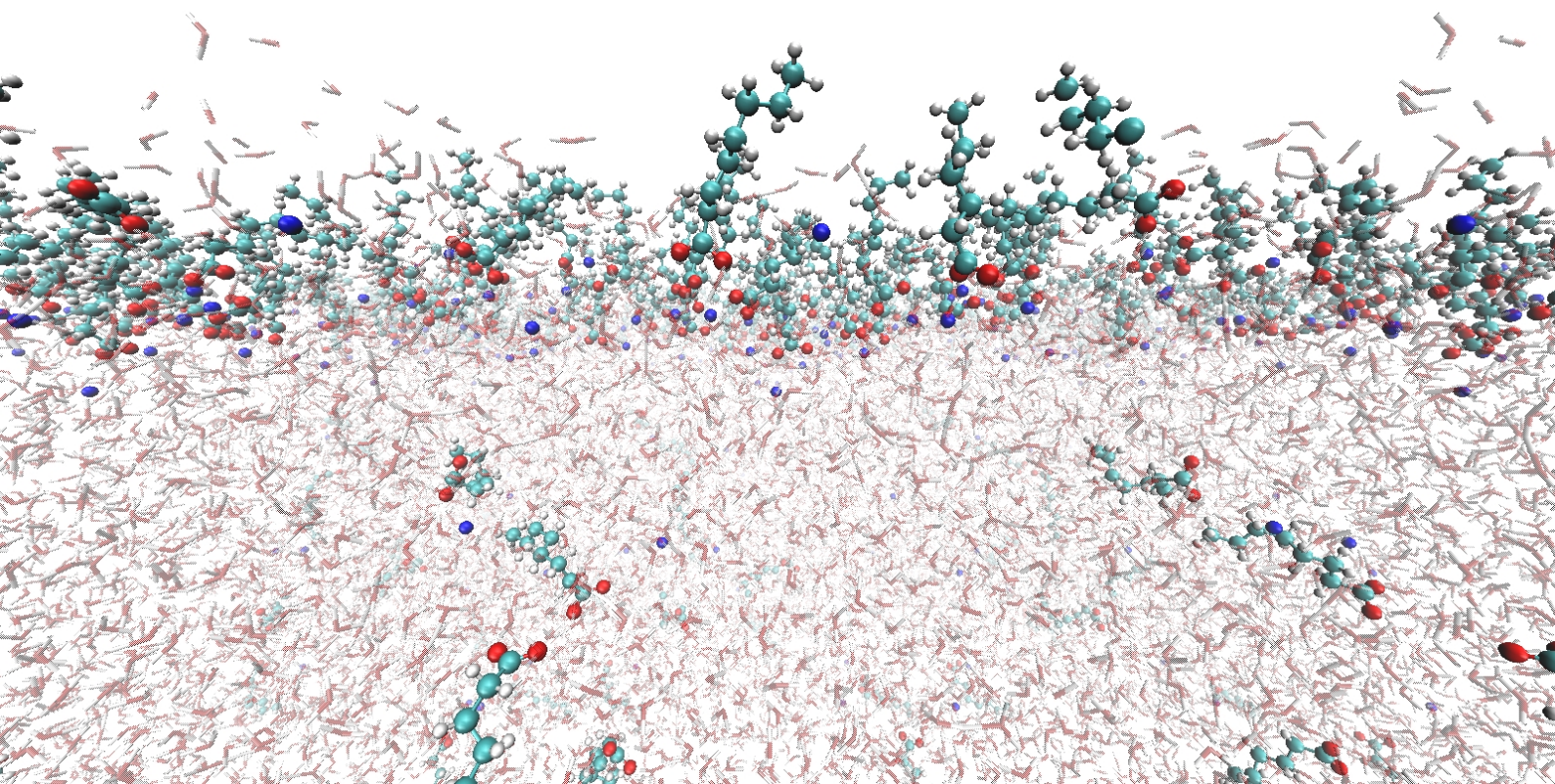


Technische Universität München
Fakultät für Chemie
Lehrstuhl für Theoretische Chemie

Modelling solvation in the liquid phase and at liquid surfaces

Jakob Filser

Dissertation





Technische Universität München
Fakultät für Chemie

Modelling solvation in the liquid phase and at liquid surfaces

Jakob Filser

Vollständiger Abdruck der von der Fakultät für Chemie der Technischen Universität München zur Erlangung des akademischen Grades eines

Doktors der Naturwissenschaften (Dr. rer. nat.)

genehmigten Dissertation.

Vorsitzender: Prof. Dr. Ulrich K. Heiz

Prüfer der Dissertation:

1. Prof. Dr. Harald Oberhofer
2. Prof. Dr. Karsten Reuter

Die Dissertation wurde am 25.04.2022 bei der Technischen Universität München eingereicht und durch die Fakultät für Chemie am 02.06.2022 angenommen.

There is no decent place to stand in a massacre.

—Leonard Cohen, *The Captain*

Den Toten des Krieges in der Ukraine.

DRAFT

Preface

This dissertation is publication-based. The scientific work associated with it is published in two peer-reviewed articles in international scientific journals. The first publication, titled *Piecewise Multipole-Expansion Implicit Solvation for Arbitrarily Shaped Molecular Solutes* was published in the *Journal of Chemical Theory and Computation*. The second publication, to which Rémi Dupuy and I contributed equally, is titled *Photoelectron angular distributions as sensitive probes of surfactant layer structure at the liquid–vapor interface* and was published in *Physical Chemistry Chemical Physics*.

DRAFT

Abstract

Modelling liquids and liquid surfaces is an issue of great interest in computational chemistry. Existing methods are matured enough for application to open scientific questions, e.g. in verifying and interpreting experimental results. At the same time, further improvement is clearly possible and desirable. State-of-the-art models can be categorized into explicit and implicit models. While the former account for the solvent in atomistic detail, the latter simulate its effect on a solute via its dielectric permittivity, plus some effects beyond classical electrostatics. In this publication based dissertation, two projects concerning such simulations are presented. In the first, a systematic error in the multipole expansion (MPE) implicit solvation model is resolved. This error arises from the expansion of the dielectric response of the solvent in an incomplete basis. Our remedy to this issue is a piecewise solution of the electrostatic problem in atom centered subregions in which the multipole basis is nearly complete. In the second publication, which is a collaboration with experimental coworkers, classical molecular dynamics simulations are employed to support advancements in the use of photoelectron angular distributions (PADs) as a probe for surface structures. The studied system is an octanoic acid surfactant on a water surface, at different concentrations and pH values. Using PADs, the qualitative surfactant structures could be determined in complete agreement with our theoretical predictions.

Zusammenfassung

Die Modellierung von Flüssigkeiten und Flüssigkeitsoberflächen ist ein Thema von großem Interesse in der theoretischen Chemie. Vorhandene Methoden sind ausgereift genug für die Anwendung auf ungeklärte wissenschaftliche Fragen, z.B. bei der Verifizierung und Interpretation experimenteller Ergebnisse. Gleichzeitig sind weitere Verbesserungen eindeutig möglich und wünschenswert. Modelle nach Stand der Wissenschaft lassen sich in explizite und implizite Modelle einteilen. Während erstere das Lösungsmittel in seiner atomaren Struktur berücksichtigen, simulieren letztere dessen Wirkung auf eine gelöste Substanz durch seine dielektrische Permittivität und zusätzlich einige Effekte über klassische Elektrostatik hinaus. In dieser publikationsbasierten Dissertation werden zwei Projekte betreffend solcher Simulationen präsentiert. Im ersten wird ein systematischer Fehler im impliziten Multipolentwicklungs-Modell (MPE) gelöst. Dieser Fehler entsteht durch die Entwicklung der dielektrischen Antwort des Lösungsmittels in einer unvollständigen Basis. Unsere Lösung für dieses Problem ist eine stückweise Lösung des elektrostatischen Problems in atomzentrierten Unterregionen, in denen die Multipolbasis annähernd vollständig ist. In der zweiten Veröffentlichung, einer Kollaboration mit experimentellen Kollegen, werden klassische Molekulardynamik-Simulationen eingesetzt um Fortentwicklungen bei der Nutzung von winkelabhängigen Verteilungen von Photoelektronen (photoelectron angular distributions, PADs) zur Bestimmung von Oberflächenstrukturen zu unterstützen. Bei den untersuchten Systemen handelt es sich um einen Oktansäure-Surfactant bei verschiedenen Konzentrationen und pH-Werten. Mittels PADs konnten die qualitativen Surfactant-Strukturen in völliger Übereinstimmung mit unseren theoretischen Vorhersagen bestimmt werden.

Contents

1 Introduction	1
2 Methods and background	5
2.1 Classical electrostatics	5
2.1.1 Microscopic behaviour	5
2.1.2 Electrostatics in condensed matter	6
2.1.3 Electromagnetic radiation	7
2.2 Quantum mechanics	7
2.2.1 Fundamentals	8
2.2.2 Hartree-Fock theory	9
2.2.3 Density functional theory	10
2.3 Thermodynamics	14
2.3.1 Ensembles and thermodynamic potentials	14
2.3.2 Thermodynamics in solution	16
2.4 Implicit solvation	17
2.4.1 The solute	17
2.4.2 The implicit solvent	18
2.4.3 The multipole expansion method	19
2.4.4 Non-electrostatic free energy contributions and parameterization	22
2.5 Classical molecular dynamics simulations	23
2.5.1 Force fields	23
2.5.2 Molecular dynamics, thermostats	25
2.5.3 Simulating surfaces	26
2.6 Experimental methods	28
2.6.1 Photoelectron spectroscopy	28
2.6.2 Photoelectron angular distributions	28
3 Publications	31
3.1 Piecewise Multipole-Expansion Implicit Solvation for Arbitrarily Shaped Molecular Solutes	33
3.1.1 Content	33
3.1.2 Individual contributions	34
3.2 Photoelectron angular distributions as sensitive probes of surfactant layer structure at the liquid-vapor interface	35
3.2.1 Content	35
3.2.2 Individual contributions	35
4 Summary, Conclusions and Outlook	37

Acknowledgments

39

Bibliography

41

DRAFT

1 Introduction

Solvents are omnipresent in chemistry. Water guides the structure and dynamics of biomolecules in living organisms.[1] Solubility is a necessary prerequisite for pharmaceuticals to take effect. The challenge of achieving said solubility has given rise to the study of drug delivery.[2] Catalytic reactions in the chemical industry are typically carried out in solution, or at the solid-liquid interface with catalytic surfaces. There, the choice of solvent can critically influence selectivity and reaction rates.[3] Despite ongoing research in the field of solid state electrolytes, state-of-the-art batteries still use liquid electrolytes.[4] Typically, non-aqueous electrolytes are required for energy-dense electrode materials. On the contrary, compatibility with aqueous electrolytes may itself be a strong enough argument to explore the capabilities of other electrode materials, to remedy the issues of toxicity and flammability in organic solvents.[5] The solvent may even be a reactant itself, e.g. in electrochemical water splitting.[6] As already hinted at by these examples, chemical and physical processes may occur in the bulk of the liquid phase, but are at least equally as commonly found at liquid-gas, liquid-liquid or liquid-solid interfaces.

As illustrated above, the solvent can rarely ever be considered an uninvolved bystander to the chemical and physical processes taking place in it. It inevitably interacts with the molecules dissolved in it and with surfaces in contact with it, influencing their physical properties and chemical behaviour. It should, thus, come as no surprise that the simulation of solvents is a fundamental challenge in computational chemistry.[3, 7–13] One might naively assume that this is a straightforward task—the electrons and nuclei of the solvent do, after all, follow the same quantum mechanical and statistical laws as those of the solute. So, if it is possible to simulate a solute from first principles, surely it must be possible to simulate a solvent, right? In an ideal world, this is certainly true. In reality, however, there is currently no computer which can accomplish this task using a reasonable amount of time and energy. The problem lies in the sheer amount of data that would be necessary. The solute is typically dilute, and it is often possible to simulate just a single molecule of it without significant loss of accuracy. The solvent, on the other hand, fills the space, and simulating a large number of solvent molecules would often be necessary to achieve converged results. The problem is further exacerbated by orders of magnitude by the issue of nuclear motion. The solvent molecules are typically small and highly mobile. Thermodynamic sampling of the combined phase space of solute and solvent would thus be necessary. Computing the full electronic structure of hundreds or thousands of atoms in thousands or millions of configurations is inefficient at best and intractable at worst.[7]

In stark contrast to this enormous effort, most of the produced data would ultimately be of little interest. Typically, one is interested only in the properties of the solute. These are largely determined by the solute's own atomistic structure. The solvent only causes a small—albeit often crucial—perturbation to these properties.[7] Even if properties of the solvent itself, such as local atomistic structure or diffusion are to be investigated, the full, quantum mechanical electronic structure of each individual solvent molecule will rarely ever be of interest.[13]

These considerations quite naturally lead to the field of solvation models. The basic idea is straightforward: Only those aspects of the solvent in which one is actually interested are accounted

for in the simulation. If the electronic structure of a solute or a surface in contact with a liquid is to be computed, then the atomistic structure of the solvent can often be ignored altogether. Instead, its time-averaged interaction with the solute is approximated in a so-called implicit solvation or continuum embedding model. [3, 7–10] On the other hand, if some property of the solvent itself, e.g. the atomistic structure of a liquid surface, is to be determined, simulating it explicitly at an atomistic level is obviously necessary. One may, however, forego calculating the full electronic structure of all atoms, instead using effective, parameterized interatomic potentials.[3, 11–13] These can also be used to simulate the solute, in cases where the electronic structure is not of interest, but rather the conformational space has to be explored.[14–16]

In implicit solvation models, the central aspect is usually the solvent's dielectric response to the electric field generated by the solute. In these models, the dielectric medium representing the solvent is assumed to fill most of the space, with the exception of a so-called cavity. The cavity represents the portion of space which is occupied by the solute, and thus inaccessible to the solvent. A wide variety of implicit solvation models following this basic recipe exist.[3, 7–10, 17–36, A1] The largest differences between them are the exact definition of the aforementioned cavity and its transition to the bulk solvent, as well as the mathematical methods used to solve the arising electrostatic problem. Free energy terms beyond classical electrostatic interactions are usually accounted for using simple empirical models, often based on effective surface tensions and, possibly, pressures.[7, 10, 17–19, A1] Other approaches do exist, but are beyond the scope of this dissertation.[8, 37]

In explicit models, on the other hand, solvent molecules are accounted for in atomistic detail. To circumvent the necessity of computing the electronic structure of the full system, the solvent and often also the solute can be approximated in a computationally cheap, fully classical description. In the simplest case, electrostatic potentials take the form of point charges located at the atomic positions.[11–13, 38] Short-range interatomic potentials arising from the quantum mechanical nature of the real atoms are approximated by pair-wise classical terms, typically taking the form of simple analytic functions. Within molecules, the complex nature of covalent bonds can be addressed by including three- and four-body terms.[13, 14] All of these terms except the electrostatic one are inherently short ranged, and their evaluation can usually be truncated at fairly short distances. The resulting method, often referred to as classical force field (FF) eliminates most of the computational effort necessary for a first principles calculation. This makes the evaluation of energies and atomic forces of a large system in many different configurations computationally tractable, facilitating applications such as molecular dynamics (MD) simulations.

As illustrated here, there are multiple aspects to consider in modelling solvation, including—but clearly not limited to—solvation in bulk liquid vs. solvation at phase boundaries and implicit vs. explicit models. Furthermore, there is the self-evident contrast between method development based on well known empirical data and application of established methods to still unanswered scientific questions. In this publication based dissertation, two separate papers are presented which explore correspondingly opposite ends of these three spectra.

In the first project, an implicit model was developed for solvation in bulk liquid.[A1] The method is an advancement of the *direct* multipole expansion (MPE) model by Sinstein *et al.*[25] In this new version, complications in the solution of the electrostatic problem are lifted, while maintaining the computational efficiency and ease of use of the original method. Results are in good agreement with established experimental reference data.[39] The method is fully integrated in the Fritz Haber Institute *ab initio* materials simulations (FHI - aims) software.[40]

In the second project, well established and computationally efficient explicit models[13, 14, 38,

41–43] were applied to aid in the confirmation and interpretation of experimental photoelectron angular distribution (PAD) data of an octanoic acid surfactant at a water surface.[A2] This data can be used to characterize the positions of atoms relative to the surface. Compared to photoelectron signal intensities at a single angle,[44] PADs are more robust to certain perturbations. Our simulations are in good agreement with experiment, helping in the establishment of this experimental technique.

Especially the first project should be viewed in the context of an ongoing effort towards an extension of the MPE method for liquid surfaces and liquid interfaces with other phases. The idea was already formulated by Markus Sinstein in his dissertation.[45] Although this will not be the first implicit solvation model for dielectric interfaces, see e.g. the work by Tomasi and coworkers[46–49], the computational efficiency and straightforward adaptation of MPE make it worth exploring the capabilities of such an extension in the near future, and progress in this direction has been made, but not yet finished, already during the work on this dissertation.

DRAFT

2 Methods and background

2.1 Classical electrostatics

The behaviour of charged particles is determined by the laws of electromagnetism. The contents of sections 2.1.1 to 2.1.3 are adapted from ref. [50] unless indicated otherwise.

2.1.1 Microscopic behaviour

A system consisting of two charged particles 1, 2 with charges Q_1, Q_2 at positions $\mathbf{r}_1, \mathbf{r}_2$ has an electrostatic potential energy

$$U = \frac{Q_1 Q_2}{\|\mathbf{r}_1 - \mathbf{r}_2\|} \quad (2.1)$$

in atomic units. This energy gives rise to the Coulomb force

$$\mathbf{F}_1 = -\nabla_1 U = -\frac{1}{2} \frac{Q_1 Q_2}{\|\mathbf{r}_1 - \mathbf{r}_2\|^3} (\mathbf{r}_2 - \mathbf{r}_1) \quad (2.2)$$

acting on particle 1, and the same force in opposite direction acting on particle 2. Here, ∇_1 is the gradient with respect to \mathbf{r}_1 .

If more than two particles are present, the forces acting on any one particle can be summed up straightforwardly. Normalizing by that particle's charge, we can obtain the electric field acting on it. It is often useful to treat the electric field as an independent quantity, without considering the charged particles that give rise to it. With only the position of the particle on which the field acts remaining as an independent variable, the index can be dropped, and we arrive at

$$\mathbf{E}(\mathbf{r}) = \frac{\mathbf{F}(\mathbf{r})}{Q} = -\nabla \frac{U(\mathbf{r})}{Q} = -\nabla \Phi(\mathbf{r}) \quad (2.3)$$

The electric field $\mathbf{E}(\mathbf{r})$ is thus the force acting on a particle of unit charge located at \mathbf{r} . Here, we have also introduced the electrostatic potential $\Phi(\mathbf{r})$ which is, correspondingly, the potential energy of a particle of unit charge located at \mathbf{r} .

If Φ is generated not by discrete point charges, but by a charge density $\rho(\mathbf{r})$, then it is given by

$$\Phi(\mathbf{r}) = \int d^3 \mathbf{r}' \frac{\rho(\mathbf{r}')}{\|\mathbf{r} - \mathbf{r}'\|} \quad (2.4)$$

and \mathbf{E} accordingly. Discrete point charges Q_i at \mathbf{r}_i can be introduced into this formalism as $\rho(\mathbf{r}) = Q_i \delta(\mathbf{r} - \mathbf{r}_i)$, using the Dirac delta distribution δ . The relation between Φ and ρ may alternatively be expressed semi-locally in the famous Poisson equation

$$\nabla^2 \Phi(\mathbf{r}) = -4\pi \rho(\mathbf{r}) \quad (2.5)$$

where ∇^2 is the Laplace operator. One important implication is that in open regions X in space which are free of charge $\rho(\mathbf{r} \in X) = 0$, Φ follows the simpler Laplace equation

$$\nabla^2\Phi(\mathbf{r}) = 0 \quad (2.6)$$

Such a potential is called a harmonic potential. A harmonic potential is uniquely defined if at every point \mathbf{r} on the boundary ∂X either Φ (Dirichlet boundary condition) or the projection of \mathbf{E} on the normal vector of the boundary (Neumann boundary condition) is known, and it is known that it has no singularities in X .

Finally, the total potential energy of a charge distribution in the absence of external fields is given by

$$U = \frac{1}{2} \int d^3\mathbf{r} \rho(\mathbf{r})\Phi(\mathbf{r}) = \frac{1}{2} \iint d^3\mathbf{r} d^3\mathbf{r}' \frac{\rho(\mathbf{r})\rho(\mathbf{r}')}{\|\mathbf{r} - \mathbf{r}'\|} \quad (2.7)$$

where the prefactor of $1/2$ arises from the fact that the interaction between charge densities at different points \mathbf{r}, \mathbf{r}' is counted twice. Using Green's first identity, the total electrostatic energy can alternatively be expressed using the electric field

$$U = \frac{1}{8\pi} \int d^3\mathbf{r} \|\mathbf{E}(\mathbf{r})\|^2 \quad (2.8)$$

2.1.2 *Electrostatics in condensed matter*

Condensed matter consists of charged or polarized particles, which follow the electrostatic laws outline above. They move around in space to minimize their free energy. With eq. (2.8), this means that they will relax to external fields in such a way that that external field is weakened. They can, however, not do this freely. These charged particles which make up matter interact with each other and have an internal structure, and displacing them increases the internal energy of the system.

External fields \mathbf{E} will thus be weakened in condensed matter, but not always completely cancelled. When working with charged particles in or near condensed media, it is oftentimes useful not to determine the displacement of every charged particle of the medium in full detail. Instead, only some charges or some charge density ρ of particular interest is treated as such. The so-called dielectric medium, on the other hand, is only considered via its effect on \mathbf{E} . It turns out that, in practice, this effect can often be described by scaling $\mathbf{E}(\mathbf{r})$ by a local, linear and isotropic factor $\varepsilon(\mathbf{r})$, called the relative dielectric permittivity. If, additionally, ε is constant, with no dependency on \mathbf{r} , the medium is called homogeneous.[45] Formally, the auxiliary quantity of the electric displacement field or flux density \mathbf{D} is introduced, which represents the electric field that ρ would produce in the absence of dielectric media.

$$\nabla\mathbf{D}(\mathbf{r}) = 4\pi\rho(\mathbf{r}) \quad (2.9)$$

The electric field is then obtained by scaling \mathbf{D} locally

$$\varepsilon(\mathbf{r})\mathbf{E}(\mathbf{r}) = \mathbf{D}(\mathbf{r}) \quad (2.10)$$

There are media and situations which do not satisfy these conditions—in fact, any medium will exhibit non-linear behaviour in the presence of strong enough \mathbf{E} —but they lie beyond the scope of this dissertation.[8]

Inserting eqs. (2.3) and (2.10) into eq. (2.9), we arrive at a generalized Poisson equation[8, 10, 36]

$$\nabla (\varepsilon(\mathbf{r})\nabla\Phi(\mathbf{r})) = -4\pi\rho(\mathbf{r}) \quad (2.11)$$

which, in the case of $\varepsilon = \text{const.} = 1$ reduces back to the already known Poisson equation (2.5).

Φ and \mathbf{D} have the useful property of being continuous even at points where ε , and therefore also \mathbf{E} are discontinuous. If ε has a sharp, step-like transition at some boundary B , e.g. the surface of a dielectric medium, then a unique solution to the electrostatic problem can be obtained by imposing continuity of the potential and the normal component of the flux density to get a unique solution (Cauchy boundary condition).[8, A1]

$$\lim_{h \rightarrow 0^+} \Phi(\mathbf{r}_B + h\mathbf{n}_B) = \lim_{h \rightarrow 0^-} \Phi(\mathbf{r}_B + h\mathbf{n}_B) \quad (2.12a)$$

$$\lim_{h \rightarrow 0^+} \mathbf{n}_B \mathbf{D}(\mathbf{r}_B + h\mathbf{n}_B) = \lim_{h \rightarrow 0^-} \mathbf{n}_B \mathbf{D}(\mathbf{r}_B + h\mathbf{n}_B) \quad (2.12b)$$

where \mathbf{r}_B are points on the boundary B and \mathbf{n}_B is the normal vector of B at \mathbf{r}_B .

2.1.3 Electromagnetic radiation

In the previous two sections, the electrostatics of resting charge carriers have been discussed. Charge carriers in motion will, in addition to the already discussed electric field \mathbf{E} , create a magnetic field \mathbf{B} . For its detailed characteristics and relation to other quantities, see e.g. ref. [50].

For the present dissertation, it is only relevant that a time-dependent \mathbf{E} is accompanied by a time-dependent \mathbf{B} . In the case of an oscillating electric field

$$\mathbf{E}(\mathbf{r}, t) = \mathbf{E}_0 \sin(\mathbf{k}\mathbf{r} - \omega t) \quad (2.13)$$

the magnetic field will oscillate accordingly

$$\mathbf{B}(\mathbf{r}, t) = \mathbf{B}_0 \sin(\mathbf{k}\mathbf{r} - \omega t) \quad (2.14)$$

forming an electromagnetic wave. The oscillation directions \mathbf{B}_0 and \mathbf{E}_0 are perpendicular to each other, as well as the propagation direction \mathbf{k} , along which the wave will propagate through space at light speed c . Electromagnetic radiation can interact with matter, transferring energy (and translational and angular momentum, which are, however, irrelevant for this dissertation). In this, the wave is quantized into photons whose energy depends on the angular frequency ω via[51]

$$E = \hbar\omega \quad (2.15)$$

with the Planck constant \hbar . Energy in the form of electromagnetic radiation of angular frequency ω can only be absorbed and released in integer multiples of this photon energy. Vice versa, if electromagnetic radiation is emitted (or absorbed) in a process which, on a microscopic level, releases (or absorbs) energy in portions of E , then the emitted (or absorbed) radiation will have an angular frequency of $\omega = E/\hbar$.

2.2 Quantum mechanics

Sections 2.2.1 and 2.2.2 are adapted from ref. [52] unless indicated otherwise.

2.2.1 Fundamentals

All matter that the field of chemistry is concerned with is composed of electrons and nuclei. These do, famously, show the characteristics of a wave rather than a particle in certain experiments. Combining classical Hamiltonian mechanics with certain relations known for the aforementioned photon, one can ultimately derive a wave equation for these particles, namely the famous Schrödinger equation.¹[51]

$$i\hbar \frac{\partial}{\partial t} |\Psi\rangle = \hat{H} |\Psi\rangle \quad (2.16)$$

Ψ is the many-body wavefunction depending on the position \mathbf{r} and the spin state s of electrons as well as nuclei. The nature of spin is of little relevance for this dissertation. Suffice it to say that it is a non-classical property of sub-atomic particles, a vector quantity with the formal dimension of an angular momentum. For the electron, the projection of this vector along any spatial coordinate always takes either of the values $\pm\hbar/2$ when measured. i is the imaginary unit. \hat{H} is the Hamilton operator. In atomic units, it is defined as

$$\hat{H} = -\frac{1}{2} \sum_i \nabla_i^2 + \sum_{i<j} \frac{1}{\|\mathbf{r}_i - \mathbf{r}_j\|} - \sum_{i,I} \frac{Z_I}{\|\mathbf{r}_i - \mathbf{R}_I\|} - \sum_I \frac{1}{2m_I} \nabla_I^2 + \sum_{I<J} \frac{Z_I Z_J}{\|\mathbf{R}_I - \mathbf{R}_J\|} \quad (2.17)$$

where \mathbf{r}_i are the electron positions and \mathbf{R}_I are the nuclear positions. Z_I and m_I are the nuclear charges and masses, respectively. ∇_i^2 is the Laplace operator of particle i . The five sums in \hat{H} describe, in order: Kinetic energy of the electrons, Coulomb interaction between the electrons, Coulomb interaction between electrons and nuclei, kinetic energy of the nuclei, and Coulomb interaction between the nuclei.

Because the nuclei are much heavier than the electrons, and are thus moving at a much longer timescale, it can in many applications be assumed that the electrons move in the potential of stationary nuclei, in the so-called Born-Oppenheimer (BO) approximation. This allows us to solve the Schrödinger equation for the electronic wavefunction only, ignoring the kinetic energy of the nuclei and the Coulomb interaction between them. These terms can later be added back in a classical picture. If, additionally, no time dependent external fields are present, the time-independent version of the Schrödinger equation can be solved instead, finally arriving at the much simplified problem

$$\hat{H}_{\text{el}} |\Psi_{\text{el},n}\rangle = E_n |\Psi_{\text{el},n}\rangle \quad (2.18)$$

with the electronic Hamilton operator

$$\hat{H}_{\text{el}} = -\frac{1}{2} \sum_i \nabla_i^2 + \sum_{i<j} \frac{1}{\|\mathbf{r}_i - \mathbf{r}_j\|} - \sum_{i,I} \frac{Z_I}{\|\mathbf{r}_i - \mathbf{R}_I\|} \quad (2.19)$$

into which the nuclear positions \mathbf{R}_I enter only as a parameter. E_n are its eigenvalues and $\Psi_{\text{el},n}$ are the corresponding eigenstates, which only depend on electronic coordinates. Since only electronic wavefunctions will be considered for the rest of this dissertation, the subscript 'el' will left out henceforth.

¹For the sake of completeness, it should be mentioned that, in principle, the Dirac equation would have to be solved. It accounts for relativistic effects, in contrast to the Schrödinger equation. Relativity is beyond the scope of this dissertation and it shall only be mentioned here that in practice, it can be approximated as a correction term, e.g. in the atom-wise scalar zeroth order regular approximation (ZORA).[40, 51]

2.2.2 Hartree-Fock theory

Electrons are fermions, which means that their wavefunction needs to fulfill the anti-symmetry condition

$$\Psi(\mathbf{x}_1, \dots, \mathbf{x}_i, \dots, \mathbf{x}_j, \dots, \mathbf{x}_{i_{\max}}) = -\Psi(\mathbf{x}_1, \dots, \mathbf{x}_j, \dots, \mathbf{x}_i, \dots, \mathbf{x}_{i_{\max}}) \quad (2.20)$$

where \mathbf{x}_i includes both the spatial position \mathbf{r}_i and the spin s_i of electron i , and i_{\max} is the number of electrons in the system. Equation (2.20) means that exchanging two electrons inverts the sign of the wavefunction. An immediate consequence of this is that two electrons of equal spin can never be in the same position, because the only way for eq. (2.20) to be fulfilled if $\mathbf{x}_i = \mathbf{x}_j$, is for Ψ to be zero. This, in turn, means that the probability of finding this state is zero, as will be discussed in section 2.2.3.

A wavefunction which satisfies this anti-symmetry by construction is given by a so-called Slater determinant

$$\Psi(\mathbf{x}_1, \mathbf{x}_2, \dots, \mathbf{x}_{i_{\max}}) = \frac{1}{\sqrt{i_{\max}!}} \begin{vmatrix} \psi_1(\mathbf{x}_1) & \psi_1(\mathbf{x}_2) & \dots & \psi_1(\mathbf{x}_{i_{\max}}) \\ \psi_2(\mathbf{x}_1) & \psi_2(\mathbf{x}_2) & \dots & \psi_2(\mathbf{x}_{i_{\max}}) \\ \vdots & \vdots & \ddots & \vdots \\ \psi_{i_{\max}}(\mathbf{x}_1) & \psi_{i_{\max}}(\mathbf{x}_2) & \dots & \psi_{i_{\max}}(\mathbf{x}_{i_{\max}}) \end{vmatrix} \quad (2.21)$$

where ψ_j are the so-called orbitals, which depend only on the coordinates of one electron. They can be calculated as eigenstates of the Fock operator \hat{f}

$$\hat{f}|\psi_i\rangle = \epsilon_i|\psi_i\rangle \quad (2.22)$$

The operator itself approximates the energy of a single electron in the system.

$$\hat{f}(\mathbf{x}) = -\frac{1}{2}\nabla^2 - \sum_I \frac{Z_I}{\|\mathbf{r} - \mathbf{R}_I\|} + \sum_j \left(\hat{J}_j(\mathbf{x}) - \hat{K}_j(\mathbf{x}) \right) \quad (2.23)$$

where here and in the following, sums of the type \sum_j are defined to run over all occupied orbitals, i.e. the orbitals that enter the Slater determinant, unless occupation numbers are stated explicitly. For the ground state manybody wavefunction, these are the i_{\max} eigenfunctions of \hat{f} with the lowest energy eigenvalues. Adaptations to this theory which use partial occupations exist, but are of no relevance for this introduction. The first two terms describe the kinetic energy of the electron and its Coulomb interaction with the nuclei. The last sum describes the interaction of one electron with the time-averaged potential generated by all other electrons. The operators \hat{J}_j and \hat{K}_j are defined by how they act on $|\psi_i\rangle$.

$$\hat{J}_j|\psi_i\rangle = \int d^3\mathbf{r}' ds' \|\psi_j(\mathbf{x}')\|^2 \frac{1}{\|\mathbf{r}' - \mathbf{r}\|} \psi_i(\mathbf{x}) \quad (2.24a)$$

$$\hat{K}_j|\psi_i\rangle = \int d^3\mathbf{r}' ds' \psi_j^*(\mathbf{x}') \frac{1}{\|\mathbf{r}' - \mathbf{r}\|} \psi_i(\mathbf{x}') \psi_j(\mathbf{x}) \quad (2.24b)$$

where ψ_j^* is the complex conjugate of ψ_j . \hat{J}_j is called the Coulomb operator and describes the time-averaged electrostatic potential generated by an electron in state $|\psi_j\rangle$. The so-called exchange operator \hat{K}_j arises from eq. (2.21) and has no classical equivalent. Nonetheless, two intuitive

conclusions can be drawn from its properties. First, for $i = j$, the terms $\hat{J}_i|\psi_i\rangle = \hat{K}_i|\psi_i\rangle$ become equal, and the corresponding element of the sum in eq. (2.23) vanishes. This means that an electron does not interact with its own electrostatic potential. Second, the integral over spin in eq. (2.24b) becomes zero if $|\psi_i\rangle$ and $|\psi_j\rangle$ have opposite spin, meaning that electrons of opposite spin interact only through the Coulomb term, like classical particles.

Despite its appearance, eq. (2.22) is thus not a simple linear problem, as \hat{f} is defined by its own eigenvectors. Therefore, it has to be solved iteratively in the so-called self-consistent field (SCF) procedure. Starting from an initial guess for the occupied orbitals $|\psi_i\rangle$, the eigenvalue problem of the arising \hat{f} operator is solved. The eigenvectors are then used to compute the next \hat{f} , the eigenvalue problem of which is solved again etc. until self-consistency is achieved.

In practice, this analytic problem is transformed into an algebraic one by a finite basis set expansion of the orbitals $|\psi_i\rangle$, and solving the generalized eigenvalue problem of the representation of \hat{f} in that basis. These technical details are not relevant for this dissertation and thus omitted.

The expectation value of the manybody Hamiltonian \hat{H} for eq. (2.21) is ultimately obtained by summation of the single electron eigenenergies ϵ_i and removing the double counting of the electron-electron interactions. This double counting arises from the fact that the interaction between electrons i and j is fully contained in both eigenvalues ϵ_i and ϵ_j . It is also useful to add the interaction between the nuclei in this step.²

$$E = \sum_i \epsilon_i - \sum_{i < j} \langle \psi_i | \hat{J}_j - \hat{K}_j | \psi_i \rangle + \sum_{I < J} \frac{Z_I Z_J}{\|\mathbf{R}_I - \mathbf{R}_J\|} \quad (2.25)$$

where the occurring vector product is defined as

$$\langle \psi_i | \hat{J}_j - \hat{K}_j | \psi_i \rangle = \int d^3\mathbf{r} ds \psi_i^*(\mathbf{x}) \left(\hat{J}_j(\mathbf{x}) - \hat{K}_j(\mathbf{x}) \right) \psi_i(\mathbf{x}) \quad (2.26)$$

2.2.3 Density functional theory

This section is adapted from refs. [40, 52] unless mentioned otherwise.

Although it may not be immediately obvious, the Hartree-Fock (HF) method outlined in the previous section is flawed in two ways: First, the representation of \hat{f} in a wavefunction basis is expensive to compute, as it requires the evaluation of double integrals over products of four wavefunctions. Second, it is an approximate method in which each electron interacts only with the time-averaged potential of all other electrons. In reality, electrons instantaneously influence each other's movement, minimizing total energy. This phenomenon is known as correlation. A rigorous treatment would require a series expansion of the manybody wavefunction in a basis of ground and excited state Slater determinants, i.e. Slater determinants into which all possible combinations of single electron orbitals enter. This method is called configuration interaction (CI) and is much more expensive than the already costly HF method. It is thus rarely used in practice. Somewhat faster approximations like Møller-Plesset perturbation theory or coupled cluster theory exist, but lie beyond the scope of this thesis. What they all have in common is that they are generally based on HF and are thus at least as computationally expensive.

²Traditionally, only the expectation values of the kinetic energy and the interaction between electrons and nuclei are summed up in the first sum, and then the double sum over electron-electron interactions is added rather than subtracted.[52] The formalism shown here is chosen because it more intuitively leads to the corresponding expression in density functional theory, shown in section 2.2.3.[40, 45]

Let us first address the issue of computational cost. In a first, straightforward adaptation to HF, the term $\sum_j \hat{J}_j$ in eq. (2.23) can be simplified. \hat{J}_j can—in contrast to \hat{K}_j —be written down explicitly without acting on a wavefunction $|\psi_i\rangle$ or using a permutation operator. The summation can then be carried out straightforwardly. The resulting quantity is a local scalar field with the dimension of an electrostatic potential.

$$\begin{aligned}\Phi_{\text{es}}(\mathbf{r}) &= \sum_j \hat{J}_j(\mathbf{r}) = \sum_j \int d^3\mathbf{r}' ds' \|\psi_j(\mathbf{x}')\|^2 \frac{1}{\|\mathbf{r}' - \mathbf{r}\|} \\ &= \int d^3\mathbf{r}' ds' \left(\sum_j \|\psi_j(\mathbf{x}')\|^2 \right) \frac{1}{\|\mathbf{r}' - \mathbf{r}\|} \\ &= \int d^3\mathbf{r}' \frac{\rho(\mathbf{r}')}{\|\mathbf{r}' - \mathbf{r}\|}\end{aligned}\tag{2.27}$$

Here, we have introduced the electron density $\rho(\mathbf{r}) = \sum_j \|\psi_j(\mathbf{r})\|^2$. In the more general case of partial occupation numbers f_j , it is defined as

$$\rho(\mathbf{r}) = \sum_j f_j \|\psi_j(\mathbf{r})\|^2\tag{2.28}$$

where the f_j sum up to the number of electrons in the system. $\rho(\mathbf{r})$ can be interpreted as the probability of finding any electron at \mathbf{r} . The spin-independent version of this formalism was used here, assuming that electrons of opposite spin occur in pairs, sharing the same spatial orbital. This assumption holds for many chemical systems. If it does not, the formalism can be generalized straightforwardly by introducing two different electron densities, one for each spin orientation.

This greatly reduces the computational cost of evaluating the interaction between $|\psi_i\rangle$ and \hat{J}_j , already highlighting the advantage of using the electron density instead of the orbitals. In fact, the latter could be replaced entirely by the density in electronic structure theory—at least in principle. The first Hohenberg-Kohn theorem—the derivation of which shall not be reiterated here—states that the ground state electron density ρ uniquely defines the electrostatic potential from sources other than electrons (usually the nuclei with given positions \mathbf{R}_I and charges Z_I), and with it the electronic Hamiltonian \hat{H} . Since \hat{H} in turn defines the electronic wavefunction and all properties of the system, this means that any chemical system can, in principle, be fully described by its ground state electron density.

In practice, however, no simple procedure or formula is known which would lead directly from ρ to the corresponding energy eigenvalue E_{tot} of \hat{H} . In particular, without a notion of individual electrons it is not straightforwardly possible to calculate their kinetic energy. As a remedy, Kohn-Sham (KS) density functional theory (DFT) takes inspiration from the HF method by computing the major part of the kinetic energy as that of a reference system of non-interacting electrons moving in the mean field of all electrons. The basic idea of KS-DFT, in contrast to the HF method, is to approximate both the computationally expensive exchange energy $-\sum_{i<j} \langle \psi_i | \hat{K}_j | \psi_i \rangle$ and the correlation energy—which is missing entirely in HF—in a functional of ρ , accordingly named the exchange-correlation (xc) functional. It is worth noting that the correlation energy, defined as the difference between the real and HF energies, also contains some kinetic contribution due to the adaptation of the electrons' movement to each other's instantaneous positions.

In the simplest case, the so-called local density approximation (LDA), the xc energy is just a functional of the electron density

$$E_{xc}[\rho(\mathbf{r})] = \int d^3\mathbf{r} \rho(\mathbf{r}) \varepsilon_{xc}(\rho(\mathbf{r})) \quad (2.29)$$

LDA produces reasonable results only for some solid state systems. For a more general applicability, more sophisticated approximations are necessary, where ε_{xc} depends also on the local density gradient $\nabla\rho(\mathbf{r})$ (generalized gradient approximation, GGA), and possibly its Laplacian $\nabla^2\rho(\mathbf{r})$ (meta-GGA)[53]. Alternatively to meta-GGA, a fraction of the exchange energy can be calculated using the HF method (hybrid functional). In the latter case, however, Φ_{xc} is no longer (semi-)local, greatly increasing the necessary computational effort. The exact functional form of ε_{xc} in any of these approximations shall not be discussed here in detail.

Apart from the such defined xc energy, KS-DFT is entirely analogous to the HF method, solving the eigenvalue problem (cf. eq. (2.22)) of a single electron operator \hat{f}_{KS} . It is worth noting that formally, the orbitals $|\psi_i\rangle$ are used only to approximate the major part of kinetic energy without assigning any real physical meaning to them. In practice, however, they are often used as approximations to the real single electron states. \hat{f}_{KS} contains the kinetic energy of the single electron moving in the mean field of all electrons, the classical electrostatic potential, and the xc interaction with all electrons

$$\hat{f}_{KS} = -\frac{1}{2}\nabla^2 + \Phi_H + \Phi_{xc} \quad (2.30)$$

Note that here, the Hartree potential Φ_H is defined to already include the potential of the nuclei, in slight contradiction to traditional DFT literature. This adjustment will make the implicit solvation formalism in section 2.4 more concise.[25]

$$\Phi_H(\mathbf{r}) = -\sum_I \frac{Z_I}{\|\mathbf{r} - \mathbf{R}_I\|} + \int d^3\mathbf{r}' \frac{\rho(\mathbf{r}')}{\|\mathbf{r}' - \mathbf{r}\|} \quad (2.31)$$

Φ_{xc} is the functional derivative of the xc functional.

$$\Phi_{xc} = \frac{\delta E_{xc}}{\delta\rho} \quad (2.32)$$

In complete analogy to the HF method, \hat{f}_{KS} is then expressed in a finite wavefunction basis, and its non-linear eigenvalue problem (cf. eq. (2.22)) is solved iteratively in the SCF procedure. The total energy is obtained by summing up the eigenvalues of the occupied single electron eigenstates, removing the double counting of the electron-electron interaction, adding the Coulomb interaction between the nuclei and replacing the interaction of the electrons with Φ_{xc} with the actual xc energy E_{xc} .

$$E[\rho] = \sum_i f_i \epsilon_i - \frac{1}{2} \int d^3\mathbf{r} \Phi_{es}(\mathbf{r}) \rho(\mathbf{r}) + \sum_{I < J} \frac{Z_I Z_J}{\|\mathbf{R}_I - \mathbf{R}_J\|} - \int d^3\mathbf{r} \Phi_{xc}(\mathbf{r}) \rho(\mathbf{r}) + E_{xc}[\rho] \quad (2.33)$$

Adding zero and rearranging eventually leads to

$$\begin{aligned}
E[\rho] &= \sum_i f_i \epsilon_i - \frac{1}{2} \int d^3\mathbf{r} \Phi_{\text{es}}(\mathbf{r}) \rho(\mathbf{r}) + \frac{1}{2} \int d^3\mathbf{r} \sum_I \frac{Z_I}{\|\mathbf{r} - \mathbf{R}_I\|} \rho(\mathbf{r}) \\
&\quad + \frac{1}{2} \sum_I \sum_J \frac{Z_I Z_J}{\|\mathbf{R}_I - \mathbf{R}_J\|} - \frac{1}{2} \sum_I \int d^3\mathbf{r} \frac{\rho(\mathbf{r})}{\|\mathbf{R}_I - \mathbf{r}\|} Z_I \\
&\quad - \int d^3\mathbf{r} \Phi_{\text{xc}}(\mathbf{r}) \rho(\mathbf{r}) + E_{\text{xc}}[\rho] \\
&= \sum_i f_i \epsilon_i - \frac{1}{2} \int d^3\mathbf{r} \Phi_{\text{H}}(\mathbf{r}) \rho(\mathbf{r}) + \frac{1}{2} \sum_I -\Phi_{\text{H}}(\mathbf{R}_I) Z_I \\
&\quad - \int d^3\mathbf{r} \Phi_{\text{xc}}(\mathbf{r}) \rho(\mathbf{r}) + E_{\text{xc}}[\rho]
\end{aligned} \tag{2.34}$$

which conveniently uses only the total classical potential Φ_{H} .

Although nuclei do, in principle, follow the same quantum-mechanical laws, the uncertainty in their position is commonly much smaller than that of electrons, due to their higher masses and consequently slower velocities. It is therefore often sufficient to approximate them as classical point charges. Within the BO approximation, $\min_{\rho} E[\rho]$ may be interpreted as a potential energy function $U(\mathbf{R}_1, \dots, \mathbf{R}_{I_{\text{max}}})$ of the nuclear positions \mathbf{R}_I on which the nuclei move. Here, we use the notation $E[\rho]$ to indicate that for the electrons, it is a total energy, including their kinetic energy, and the notation $U(\mathbf{R}_1, \dots, \mathbf{R}_{I_{\text{max}}})$ to indicate that for the nuclei, it is a potential energy, missing their kinetic energy. In practice, the former is the way in which the latter is evaluated; the different notations only hint at the different interpretations of this quantity in different steps of the calculation.

Let us finally briefly address the issue of SCF convergence. Simply filling the orbitals of lowest energy in each step would lead to slow convergence of the algorithm, or no convergence at all. Therefore, various adaptations are made in guessing the electron density from which eq. (2.30) is computed for the next step. Elaborating on these in detail lies beyond the scope of this thesis. Suffice it to say that they generally fall into either of two categories: First, the occupation of the energetically higher lying orbitals is ‘broadened’, with some orbitals around the energy boundary between occupied and unoccupied orbitals being partially occupied. Second, fluctuations in the electron density between SCF iterations are dampened, ‘mixing’ some of the solutions from previous iterations with the solution of the current step. This means that the density used to construct the next \hat{f}_{KS} is not actually constructed from the eigenvectors of the current \hat{f}_{KS} , and solving eq. (2.34) for these not self-consistent quantities would constitute additional computational work. Since the procedure is only terminated once relative self-consistency is achieved anyway, and the not self-consistent total energy in SCF steps before convergence is of little interest, an approximation can be employed in the so-called Harris functional. It has the same structure as eq. (2.33)—and shall therefore not be repeated here explicitly—but only the single electron energy eigenvalues are taken from the solution to the current \hat{f}_{KS} , whereas all other terms are evaluated using the mixed electron density which was used to construct \hat{f}_{KS} . It thus uses only terms which are computed anyway, making the method computationally efficient while still converging to the same value in the limit of self-consistency.

2.3 Thermodynamics

The Hamiltonian eq. (2.17) uniquely defines the behaviour of the described system in isolation.[51] The calculation of macroscopic quantities from this information is, however, not straightforward. The fields of thermodynamics³ and statistical mechanics deal with this task. The contents of section 2.3.1 are adapted from refs. [54–57] unless indicated otherwise.

2.3.1 Ensembles and thermodynamic potentials

Generally, a system of fixed composition can exchange energy with its environment either as heat δQ or work δW , expressed in the first law of thermodynamics

$$dE = \delta Q + \delta W \quad (2.35)$$

Note that the total energy is a state function, indicated by the notation dE , whereas heat δQ and work δW depend on the path through the system's phase space. Work can be performed in different ways, the simplest of which is volume expansion dV against an external pressure p .

$$\delta W = -p dV \quad (2.36)$$

Heat refers to any energy transfer that is not work and it is generally associated with a change in temperature T , which in turn is associated with thermal motion of particles. In the absence of any non-volume work, the differential of the inner energy becomes

$$dE = \delta Q - p dV \quad (2.37)$$

If all terms in the above equation are zero, i.e. if the system's energy is strictly conserved and its volume is kept constant, then statistical predictions such as expectation values of observables in such a system can be made based on a so-called microcanonical ensemble. An ensemble is a theoretical construct consisting of copies of the system which are physically identical in certain fixed quantities. Each copy occupies a different microstate (i.e. values for the positions and momenta of all particles) that is possible under these constraints. Together, the copies explore all possible microstates. The ergodic hypothesis states that the ensemble average of any observable is equal to its time average over sufficiently long time.⁴

In the case of the microcanonical ensemble, we explicitly defined that V and E are constant. Additionally, we implicitly assumed that the number of particles N is constant. The microcanonical ensemble is thus defined by these three quantities, and is accordingly also known as NVE ensemble.

δQ is not itself a state function. Surprisingly, if the associated process is reversible, it can nonetheless be expressed as the differential of a state function by normalizing by the temperature T . That state function is called the entropy S .

$$dS = \frac{\delta Q}{T} \quad (2.38)$$

Most people consider this definition to be somewhat unintuitive to interpret. More straightforwardly, S is often described as a measure for disorder.

³or kinetics, if the system's macroscopic properties change over time and/or there is a non-zero net flux of matter and/or energy in and out of it

⁴It does, however, not make any assertions about what time is sufficiently long.

Since we defined that in the microcanonical ensemble $\delta Q = 0$, we can easily see that in equilibrium $dS = 0$, i.e. S has a stationary point, specifically a maximum. The exact derivation involves also considering irreversible processes and shows that S is not strictly constant like N , V and E , but only reaches its maximum in equilibrium. For the sake of brevity, this derivation is left out here.

We have seen that the behaviour of the microcanonical ensemble is driven by the maximization of entropy. S is therefore also called the thermodynamic potential of the microcanonical ensemble. The latter is useful for theoretical considerations due to its simplicity. In practical experiments, however, one is more frequently dealing with system which can exchange heat and/or volume or particles with their environment.

Let us first consider a system which can exchange heat with a surrounding heat bath of temperature T , but cannot expand/contract or exchange particles with the environment. If the heat bath is sufficiently large that its temperature does not change in the process, and the coupling between system and heat bath is sufficiently strong that the system reaches the same T in equilibrium, then the corresponding ensemble is defined by NVT . It is also known as the canonical ensemble.

Using eqs. (2.37) and (2.38), we can write the differential of the inner energy for reversible processes using only state functions.⁵

$$dE = T dS - p dV \quad (2.39)$$

We can use a Legendre transformation to shift the dependence from S to T and define the thermodynamic potential of the canonical ensemble, called the Helmholtz free energy

$$F = E - TS \quad (2.40)$$

with its total differential

$$dF = dE - T dS - S dT = -p dV - S dT \quad (2.41)$$

Like dS in the microcanonical ensemble, dF becomes zero for reversible processes in the canonical ensemble, and the behaviour of the ensemble is driven by F approaching its stationary point, in this case its minimum.

If additionally the particles are not confined to a static volume, then depending on the specific situation one may describe this phenomenon either as the system expanding/contracting, or exchanging particles with its environment. Using both descriptions simultaneously makes little sense in most cases, as it would require some definition of whether particle movement at the system boundary is to be interpreted as volume change or particle exchange, which is usually not straightforward.

If the system is exposed to an environment of constant pressure and can change its volume to reach the same internal pressure, then the thermodynamic potential of the resulting NpT ensemble is the Gibbs free energy, sometimes also called free enthalpy

$$G = F + pV \quad (2.42)$$

⁵The average inner energy of an ensemble is often denoted as U rather than E , which is used for the energy of an individual microstate. Generally, both quantities are equal only in the microcanonical ensemble. Nonetheless, for the sake of consistency with the rest of this thesis, we use E for the inner energy here.

whose total differential

$$dG = dF + p dV + V dp = -S dT + V dp \quad (2.43)$$

becomes zero for reversible processes in the NpT ensemble, meaning that G is minimized in equilibrium.

The case of a system of constant volume exchanging particles with its environment is described in the grand-canonical ensemble, but lies beyond the scope of this thesis.

2.3.2 Thermodynamics in solution

Bridging the gap between theory and experiment, it is necessary to choose a quantity which can be determined both ways, allowing for a comparison. In the case of solvation, the free energy of solvation ΔG_{solv} in the limit of infinite dilution is a straightforward choice. It is defined as the Gibbs free energy necessary for (or released by, in the common case of a negative sign) moving a single solute molecule from vacuum into bulk solvent at constant temperature and pressure. ΔG_{solv} of neutral solutes is commonly computed from partition coefficients P —i.e. concentration ratios—of the solute between gas phase and solution, or between solution and some other reference solvent for which the solute's partition coefficient with the gas phase is known.[19] The free energy of solvation can be obtained as

$$\Delta G_{\text{solv}} = -k_{\text{B}}T \ln(P) \quad (2.44)$$

with the Boltzmann constant k_{B} . This well-known condition concerning chemical equilibrium can be derived from first principles using the definitions from the previous section. The detailed proof is, however, lengthy, and the reader is once again referred to the extensive literature on this subject.[54] For ionic solutes, the fact that G is a state function can be exploited in thermodynamic cycles.[58]

The thermodynamic system comprises just the solute molecule, treating the solvent as its environment. There is, so far, no approximation in this definition, as long as all interactions are accounted for exactly. Assuming that all pressure arises from the solvent, the internal Gibbs and Helmholtz free energies of the solute become equivalent. The Gibbs free energy of the solute in solution can then be decomposed into[8, 10]

$$G_{\text{solv}}[f_1(\mathbf{X}_{\text{solute}}), f_2(\mathbf{X}_{\text{solvent}})] = G_{\text{solute}}[f_1(\mathbf{X}_{\text{solute}})] + \Delta G_{\text{inter}}[f_1(\mathbf{X}_{\text{solute}}), f_2(\mathbf{X}_{\text{solvent}})] \quad (2.45)$$

The first term contains the free energy of the solute and the second one contains its interaction with the solvent. $\mathbf{X}_{\text{solute/solvent}}$ are any applicable degrees of freedom (DOF) of the solute and solvent, and $f_{1/2}$ are their respective distributions in thermodynamic equilibrium. The Δ indicates that all contributions to this term are differences to a reference state consisting of the unperturbed bulk solvent and the solute in vacuum. The internal energy of the solvent is not included here, as it is not part of the ensemble. However, although not denoted explicitly, ΔG_{inter} does contain the difference of this internal energy compared to the unperturbed bulk solvent. The free energy of solvation is defined as

$$\Delta G_{\text{solv}} = G_{\text{solv}} - G_{\text{vac}} = G_{\text{solute}} - G_{\text{vac}} + \Delta G_{\text{inter}} \quad (2.46)$$

where G_{solv} is the free energy in solution as defined in eq. (2.45) at infinite dilution and at a given T and p , and G_{vac} is the free energy in gas phase at the same T and at $p = 0$, i.e. that of a single molecule in vacuum. With these definitions in place, we can now turn our attention to the computation of the individual terms, which will be addressed in the following sections.

2.4 Implicit solvation

2.4.1 The solute

Exact evaluation of eq. (2.45) would involve an integration over both solute and solvent degrees of freedom, requiring considerable—if not intractable—computational effort. It is therefore necessary to make approximations.

Let us decompose the terms in eqs. (2.45) and (2.46) further. Within the scope of the BO approximation, the internal free energies of the solute $G_{\text{solute/vac}}$ both in solution and in vacuum consist of the expectation values of the potential energy U and kinetic energy E_{kin} of the nuclei, as well as an entropic contribution.[10] Again, we made the assumption that the solute has no internal pressure, and the Helmholtz and Gibbs free energies are therefore equivalent.

$$G_{\text{solute/vac}} = \langle U(\mathbf{R}_1, \dots, \mathbf{R}_{I_{\text{max}}}) \rangle + \langle E_{\text{kin}} \rangle - T \langle S \rangle \quad (2.47)$$

In a first approximation concerning the solute degrees of freedom, we can now assume that the kinetic and entropic contributions can be neglected. Although this appears to be a quite radical simplification at first, in the context of ΔG_{solv} it only assumes that

$$|\Delta \langle E_{\text{kin}} \rangle - T \Delta \langle S \rangle| \ll |\Delta \langle U \rangle + \Delta G_{\text{inter}}| \quad (2.48)$$

where all Δ refer to differences between solution and gas phase. In other words, we assume that ΔG_{solv} is dominated by the change in the solute's internal potential energy and its interaction with the solvent rather than the change in its thermal motion. Next, we can approximate

$$\begin{aligned} \Delta \langle U \rangle &= \langle U_{\text{vac}}(\mathbf{R}_1, \dots, \mathbf{R}_{I_{\text{max}}}) \rangle - \langle U_{\text{solute}}(\mathbf{R}_1, \dots, \mathbf{R}_{I_{\text{max}}}) \rangle \\ &\approx U_{\text{vac}} \left(\operatorname{argmin}_{U_{\text{vac}}}(\mathbf{R}_1, \dots, \mathbf{R}_{I_{\text{max}}}) \right) - U_{\text{solute}} \left(\operatorname{argmin}_{U_{\text{solute}} + \Delta G_{\text{inter}}}(\mathbf{R}_1, \dots, \mathbf{R}_{I_{\text{max}}}) \right) \end{aligned} \quad (2.49)$$

where $\operatorname{argmin}_a b$ is the value of b that minimizes $a(b)$, U_{vac} is the nuclear potential energy obtained from the self-consistent electronic structure in vacuum, and U_{solute} is the same quantity in solution.[8] Again, the central assumption is that energy differences due to different movement of the nuclei around the potential energy minima are small compared to energy differences due to the minima themselves. In practice, these energies can be calculated to reasonable accuracy using DFT, cf. section 2.2.3. How the presence of a solvent impacts the electronic structure will be discussed in the following sections. Lastly, we can approximate

$$\operatorname{argmin}_{U_{\text{solute}} + \Delta G_{\text{inter}}}(\mathbf{R}_1, \dots, \mathbf{R}_{I_{\text{max}}}) \approx \operatorname{argmin}_{U_{\text{vac}}}(\mathbf{R}_1, \dots, \mathbf{R}_{I_{\text{max}}}) \quad (2.50)$$

If U_{vac} and U_{solute} are computed from converged electronic structures in vacuum and in solution, respectively, then they are not equal even if they are evaluated at the same nuclear geometry. The reason for treating the electronic structure self-consistently, but not the geometry, is of rather practical nature: In DFT, computing the electronic structure in solution is computationally cheap, as it requires going through the SCF procedure only once. Obtaining the relaxed geometry $\operatorname{argmin}_{U_{\text{solute}} + \Delta G_{\text{inter}}}(\mathbf{R}_1, \dots, \mathbf{R}_{I_{\text{max}}})$, on the other hand, requires an unpredictable number of SCF procedures, as the energy needs to be minimized in an iterative optimization of the geometry, requiring a full electronic SCF calculation at each step. Using the vacuum geometry[19, 59], or more

generally some estimate $(\mathbf{R}_1, \dots, \mathbf{R}_{I_{\max}}) \Big|_{\text{est}}$ for both calculations thus reduces the computational time significantly. With these approximations now in place, eq. (2.46) becomes[25]

$$\Delta G_{\text{solv}} = U_{\text{solute}} \left((\mathbf{R}_1, \dots, \mathbf{R}_{I_{\max}}) \Big|_{\text{est}} \right) - U_{\text{vac}} \left((\mathbf{R}_1, \dots, \mathbf{R}_{I_{\max}}) \Big|_{\text{est}} \right) + \Delta G_{\text{inter}} + \Delta G_{\text{nuc}} \quad (2.51)$$

The correction term ΔG_{nuc} introduced here contains all errors due to approximations so far, namely the free energy difference due to thermal motion of the solute nuclei[8] and the error introduced in eq. (2.50).

2.4.2 The implicit solvent

Let us now turn to the parts of eq. (2.51) that we have not touched yet, $\Delta G_{\text{inter}} + \Delta G_{\text{nuc}}$. As indicated in eq. (2.45), exact evaluation of the first term would involve an integration over the degrees of freedom of the solvent particles. The central idea of implicit solvation methods is to model the solvent as a structureless dielectric medium, ignoring individual solvent particles and making an integration over their degrees of freedom obsolete.[8]

We can apply the ultimate approximation from the previous section to $\Delta G_{\text{inter}} + \Delta G_{\text{nuc}}$, representing it as a function of a single nuclear geometry. This further reduces the degrees of freedom that need to be considered. It should be pointed out that this is not an inherent part of implicit solvation models. For example, it is possible with such models to actually carry out geometry relaxation in solution, simulate the molecular dynamics of the solute (cf. section 2.5.2), or compute the solvent effect on vibrational spectra.[8, 18] Nonetheless, the approximation of a single geometry will be applied in the following throughout, as it lifts the necessity of distinguishing between model terms evaluated at given nuclear geometries and their thermodynamic average counterparts.

Implicit solvation models commonly separate ΔG_{inter} into two terms. The first is the mean-field electrostatic interaction ΔG_{mf} between the solute and the solvent, represented as a dielectric continuum. Free energy contributions that do not fall into this first term can be summarized with ΔG_{nuc} in a non-electrostatic model term $\Delta G_{\text{solv}}^{\text{non-elstat}}$ which is typically more empirical in design.[10, 25]

$$\Delta G_{\text{inter}} + \Delta G_{\text{nuc}} = \Delta G_{\text{mf}} + \Delta G_{\text{solv}}^{\text{non-elstat}} \quad (2.52)$$

The free energy of solvation is thus calculated as

$$\Delta G_{\text{solv}} = \underbrace{U_{\text{solute}} + \Delta G_{\text{mf}}}_{E_{\text{solv}}[\rho]} - \underbrace{U_{\text{vac}}}_{E_{\text{vac}}[\rho]} + \Delta G_{\text{solv}}^{\text{non-elstat}} \quad (2.53)$$

In a DFT context, U_{vac} is calculated as the electronic ground state energy in vacuum $E_{\text{vac}}[\rho]$, as described in section 2.2.3. U_{solute} and ΔG_{mf} are computed together as the electronic ground state energy $E_{\text{solv}}[\rho]$ from a DFT calculation where the classical electrostatic potential Φ_{H} is corrected by the dielectric response of the solvent, as will be elaborated in the following.[8, 25] $\Delta G_{\text{solv}}^{\text{non-elstat}}$ will be addressed in section 2.4.4.

For $E_{\text{solv}}[\rho]$ to be uniquely defined, the dielectric medium representing the solvent needs to be defined. Typically, it is modelled by a local, linear and isotropic relative permittivity $\varepsilon(\mathbf{r})$.[10,

45] For portions of space that are far separated from the solute, ε assumes the experimentally known macroscopic permittivity $\varepsilon_{\text{bulk}}$ of the solvent in question. Space occupied by the solute, on the other hand, needs to be assumed to be free of solvent. This is modelled as a so-called ‘cavity’ around the solute. Inside the cavity, $\varepsilon = 1$. Any dielectric effects in this region are accounted for explicitly at the DFT level. Between the cavity and the bulk solvent, ε can be modelled either as a continuous function of \mathbf{r} , [18, 20–22] or as a piecewise constant function with a step transition at a sharp cavity boundary. [8, 19, 23–25] While both variants have found numerous practical implementations—clearly not limited to those cited here—continuous permittivities lie beyond the scope of the present thesis. Ultimately, comparable models using continuous [18] and piecewise constant [25] permittivities yield similar agreement with experimental reference ΔG_{solv} .

Various definitions for the location of the cavity boundary are possible. In the context of DFT, a natural choice is an isosurface of the solute electron density, as it is readily available and follows the shape of the solute. [25, A1]

$$\varepsilon(\mathbf{r}) = \begin{cases} 1, & \rho(\mathbf{r}) > \rho_{\text{iso}} \\ \varepsilon_{\text{bulk}}, & \rho(\mathbf{r}) < \rho_{\text{iso}} \end{cases} \quad (2.54)$$

With this definition in place, a DFT calculation in implicit solvent is conducted by replacing Φ_{H} in eqs. (2.30) and (2.34) with a classical potential Φ which fulfills eq. (2.12) at the cavity boundary and eq. (2.11) inside the cavity and in the solvent.

2.4.3 The multipole expansion method

With the dielectric medium that represents the solvent defined and the equations for the electrostatic potential formulated, the computational challenge now lies in actually solving these equations in a way that allows for $\Phi(\mathbf{r})$ to be evaluated at arbitrary positions in space \mathbf{r} , which will allow us to perform the DFT calculation. Different approaches to this task have been developed and applied. In ref. [A1] we focus on the so-called multipole expansion (MPE) method.

The Poisson equation (2.5) defining Φ_{H} and the generalized Poisson equation (2.11) defining the total classical potential Φ become equivalent inside the cavity where $\varepsilon = 1$. This means that the difference between the two, called the reaction field Φ_{R} , [25, 31] needs to fulfill the Laplace equation (2.6).

$$\nabla^2 \Phi_{\text{R}}(\mathbf{r}) = \nabla^2 (\Phi(\mathbf{r}) - \Phi_{\text{H}}(\mathbf{r})) = 0 \quad (2.55)$$

Φ_{R} is thus a so-called harmonic potential. As already mentioned in section 2.1.1, harmonic functions are uniquely defined in open regions in space if certain conditions on the region boundary are known. [50] If that region is strictly convex, a complete basis for continuous harmonic functions is given by the regular solid harmonics [A1]

$$\mathcal{R}_m^l(\mathbf{r}) = r^l Y_m^l(\theta, \phi) \quad , \quad l = 0, 1, \dots \quad , \quad m = -l, -l+1, \dots, l \quad (2.56)$$

where (r, θ, ϕ) is \mathbf{r} in spherical coordinates, and Y_m^l are the spherical harmonic functions or their real-valued linear combinations. [40] Φ_{R} may thus be expanded in this basis [25, 32, 34]

$$\Phi_{\text{R}}(\mathbf{r}) = \sum_{l,m} R_K^{(l,m)} \mathcal{R}_m^l(\mathbf{r} - \mathbf{r}_K) \quad (2.57)$$

with expansion coefficients $R_K^{(l,m)}$ and some expansion center \mathbf{r}_K . In practice, Φ_R can often—but not always, as we will discuss—be approximated to reasonable accuracy in this way even if the region with $\varepsilon = 1$, i.e. the cavity, is not convex. Furthermore, the expansion has to be truncated at a finite order l_{\max} for practical applications. \mathcal{R}_m^l may be thought of as potentials inside a sphere, generated by multipole-like charge distributions on that sphere, hence the name multipole expansion.

If a different cavity definition than eq. (2.54) is chosen such that the solute charge density is entirely confined in it, i.e.

$$\rho(\mathbf{r}) = 0 \quad \forall \mathbf{r} : \varepsilon(\mathbf{r}) \neq 1 \quad (2.58)$$

then Φ fulfills the Laplace equation outside the cavity, too. Imposing the condition that it approaches zero for large \mathbf{r} , it cannot be expanded in \mathcal{R}_m^l . Rather than that, it has to be expanded in the irregular solid harmonics[34]

$$\mathcal{I}_m^l(\mathbf{r}) = r^{-(l+1)} Y_m^l(\theta, \phi) \quad , \quad l = 0, 1, \dots \quad , \quad m = -l, -l+1, \dots, l \quad (2.59)$$

Based on ideas[30, 31] that predate computational chemistry (and, in fact, computers in a modern sense altogether), early applications of the MPE method to electronic structure calculations[32, 34, 35] decomposed the solute charge density ρ into multipole moments and computed the expansion coefficients of Φ_R and of Φ outside the cavity using their relation to these solute multipole moments. A great drawback of these methods was that they relied on eq. (2.58). If solute charge lied outside the cavity, the electrostatic potentials would suffer from a thusly named outlying charge error. Simulating the strong solute-solvent interaction in polar solvents like water does, however, require fairly ‘tight’ cavities where the model dielectric overlaps with the solute charge.[25, A1]

This outlying charge error is resolved in the so-called direct method by Sinstein *et al.*[25]. At its core, it generalizes the ansatz for the electrostatic potential inside the cavity in a way that can also be applied outside of it.

$$\Phi(\mathbf{r}) = \varepsilon^{-1}(\mathbf{r})\Phi_H(\mathbf{r}) + \Phi_{\text{MPE}}(\mathbf{r}) \quad (2.60)$$

where inside the cavity, Φ_{MPE} is the reaction field Φ_R and outside it is called Φ_Q . In order for Φ_{MPE} to be harmonic, it is sufficient that ε is constant; eq. (2.58) is no longer required. In analogy to eq. (2.57), Φ_Q is expanded in the irregular solid harmonics

$$\Phi_Q(\mathbf{r}) = \sum_J \sum_{l,m} Q_J^{(l,m)} \mathcal{I}_m^l(\mathbf{r} - \mathbf{r}_J) \quad (2.61)$$

with expansion centers \mathbf{r}_J placed on the positions of the solute nuclei. With eq. (2.60), the dielectric boundaries conditions eq. (2.12) become

$$\begin{aligned} \Phi_R(\mathbf{r}) - \Phi_Q(\mathbf{r}) &= \left(\varepsilon_{\text{bulk}}^{-1} - 1 \right) \Phi_H(\mathbf{r}) \\ \mathbf{n}_r \nabla \left(\Phi_R(\mathbf{r}) - \varepsilon_{\text{bulk}} \Phi_Q(\mathbf{r}) \right) &= 0 \end{aligned} \quad (2.62)$$

where \mathbf{n}_r is the normal vector of the cavity surface at \mathbf{r} . Inserting eqs. (2.57) and (2.61), truncated at finite expansion orders into eq. (2.62) and evaluating at a finite set of points at the cavity boundary allows us to represent these boundary conditions in a system of linear equations. The

solution to this system contains the expansion coefficients $R_K^{(l,m)}$, $Q_J^{(l,m)}$, in turn allowing for evaluation of eq. (2.60) at arbitrary \mathbf{r} .

Although the direct method enabled the application of the MPE method regardless of the relation between cavity and solute shape, it did not yet address the cavity shape itself. As mentioned earlier, the expansion of Φ_R in \mathcal{R}_m^l converges with expansion order if the cavity is strictly convex. In ref. [A1] we show that for some non-convex cavities the expansion does not converge efficiently, and sometimes not at all. Such cavity shapes are, however, commonly found when applying isodensity cavities in the fashion of eq. (2.54) to large molecular solutes, necessitating further refinement of the method.

We address this issue in the same publication by separating the cavity into nearly convex subregions centered around the non-hydrogen nuclei of the solute. Previously, a very similar adaptation[26–28] has been successfully applied to the conductor-like screening model (COSMO)[23]. In our method, Φ_R is expanded in the fashion of eq. (2.57), but—in contrast to the previous version[25]—with each region K having its own set of expansion coefficients $R_K^{(l,m)}$ (and its own expansion center \mathbf{r}_K which is, however, irrelevant at finite expansion orders due to the translational properties[60, 61] of \mathcal{R}_m^l). Just like in Sinstein’s method, the cavity surface is discretized as illustrated in fig. 2.1 and the multipole expansions are inserted into eq. (2.62), evaluated at these points. In our case, $\Phi_R(\mathbf{r})$ is taken to be the multipole series of whichever subregion of the cavity is in contact with \mathbf{r} . Equivalent conditions are imposed at discrete points at the boundaries between the subregions, yielding the relations between the multipole expansions in these regions. Ultimately, a system of linear equations which can be solved for the expansion coefficients is obtained, in complete analogy to ref. [25]. We showed that with this adaptation the multipole expansion reliably converges to reasonable accuracy at an expansion order of $l_{\max} = 8$ for the potentials inside the cavity subregions.

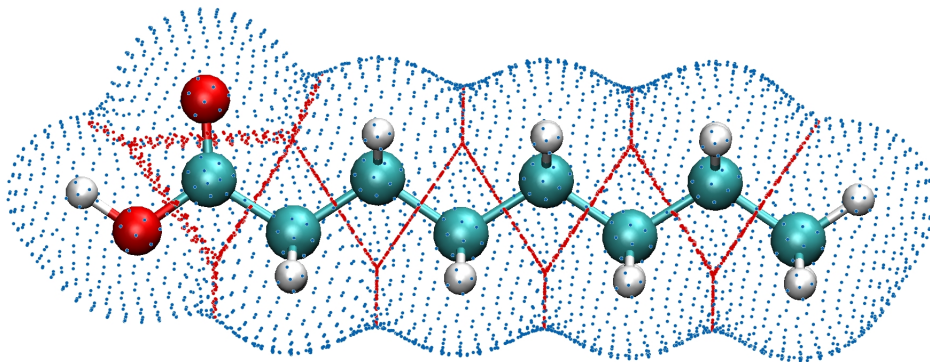


Fig. 2.1: Octanoic acid molecule with discretized cavity surface (blue) and boundaries between cavity subregions (red).

2.4.4 Non-electrostatic free energy contributions and parameterization

Let us now finally disentangle the free energy terms not covered by the dielectric model which so far were summarized in $\Delta G_{\text{solv}}^{\text{non-elstat}}$. By definition, it consists of those parts of ΔG_{inter} which are not captured in the electrostatic model, and of ΔG_{nuc} .

The first part is dominated by the cavity formation or cavitation free energy, i.e. free energy due to the displacement of solvent molecules by the solute, forming the cavity. It would be fully described by the solvent's surface tension if the solute-solvent interface was sufficiently smooth and planar and pressure could be neglected. Neither of these assumptions is necessarily fulfilled, and for cavities on molecular length scales, the cavitation energy is actually linearly correlated with the cavity volume rather than its surface area.[62] Nonetheless, an effective surface tension is a reasonable approximation even in this case.[17]

Another part of ΔG_{inter} is due to the quantum mechanical nature of the electrons of both the solute and the solvent. It can be further decomposed into Pauli repulsion and dispersive interactions. Both interactions are inherently short ranged. It can thus be assumed that they act primarily at the cavity surface.[10]

The model which we will use below depends on a single solute geometry. This is seemingly incompatible with the notion of it containing terms due to nuclear motion ΔG_{nuc} . The model may, however, be interpreted to take as an input the equilibrium solute geometry or an estimate of it—cf. eqs. (2.49) and (2.50) and accompanying considerations in section 2.4.1—and yield as an output the free energy due to relaxation and changed thermal motion around that geometry.

As we have seen, all contributions to $\Delta G_{\text{solv}}^{\text{non-elstat}}$ either depend on the cavity surface area explicitly or can be assumed to originate mostly from interactions at the surface, except ΔG_{nuc} and the cavitation term. The latter may, however, at least be approximated by a dependence on the surface area. This naturally leads to the idea of modelling this energy using an effective surface tension. This may be done either by assigning different surface tensions to different parts of the cavity, taking the solute into account[19], or by using just a single effective surface tension which depends only on the solvent.[18] In ref. [A1] we used the latter.

$$\Delta G_{\text{solv}}^{\text{non-elstat}} = \alpha A \tag{2.63}$$

where A is the total area of the density isosurface $\{\mathbf{r} : \rho(\mathbf{r}) = \rho_{\text{iso}}\}$ defining the cavity boundary, cf. eq. (2.54), and α is a solvent specific empirical parameter with the dimension of a surface tension.

Similar methods additionally assign an effective pressure to the solvent, which is multiplied with the cavity volume.[18, 25] It has, however, been found that for molecular solutes this volume is strongly linearly correlated with the cavity surface area. The effective pressure may thus even be chosen freely if the effective surface tension is determined accordingly.[59] In our work, we found no significant improvement regarding agreement with experiment by inclusion of a volume dependent term. We therefore used eq. (2.63) throughout.

Although describing $\Delta G_{\text{solv}}^{\text{non-elstat}}$ by just a single solvent dependent effective surface tension is clearly an oversimplification, this model can achieve reasonable agreement with experiment. The advantage of such a simplistic model is that the possibility of overfitting is almost certainly ruled out. Our version of the MPE method uses only three physical model parameters, ϵ_{bulk} , ρ_{iso} and α , the first of which is experimentally known for commonly used solvents.

This leaves us with only two parameters which need to be fitted to experimental reference data. To this end we employ the Minnesota Solvation Database.[39] It contains ΔG_{solv} of small

molecules in different solvents. In our work we restricted ourselves to water as a solvent. Explicitly denoting the dependence on these parameters, our calculated free energy of solvation according to eq. (2.53) is

$$\Delta G_{\text{solv}}^{\text{calc}}(\rho_{\text{iso}}, \alpha) = \Delta G_{\text{solv}}^{\text{elstat}}(\rho_{\text{iso}}) + \alpha A(\rho_{\text{iso}}) \quad (2.64)$$

where $\Delta G_{\text{solv}}^{\text{elstat}}$ is the difference between the solute's ground state energies in dielectric medium and in vacuum. Minimizing the root mean square error of eq. (2.64) with respect to experimental values yields an optimized set of $\rho_{\text{iso}}, \alpha$.

The properties of ΔG_{nuc} were not taken into account when choosing eq. (2.63) as a functional form for $\Delta G_{\text{solv}}^{\text{non-elstat}}$. In fact, the former was originally not considered to be part of the latter.[18] In practice, however, it is to some degree accounted for when fitting α to experimental ΔG_{solv} , which inevitably contain ΔG_{nuc} . [A1]

Remarkably, already the single cavity model of Sinstein *et al.*[25] achieved approximately the same agreement with experiment as our modified method. This is due to the reference data being biased towards very small solute molecules, where convergence of the multipole series for Φ_{R} is generally unproblematic. Additionally, considering that both terms are fit together to a single observable, the experimental solvation free energy, systematic errors in $\Delta G_{\text{solv}}^{\text{elstat}}$ may be compensated for by systematic errors in $\Delta G_{\text{solv}}^{\text{non-elstat}}$. However, there is no guarantee that this error cancellation can be extrapolated to arbitrary solute shapes and sizes. Our modified method resolves this issue by not relying on such error cancellation in the first place. [A1]

2.5 Classical molecular dynamics simulations

2.5.1 Force fields

The computational cost of calculating $U(\mathbf{R}_1, \dots, \mathbf{R}_{I_{\text{max}}})$ using the methods discussed so far is dominated by the electronic structure or DFT calculation. If one is interested only in the nuclear geometry, it may seem disproportionate to invest much computational time in calculating an electronic structure in which one is ultimately not interested. It would seem much more reasonable to express U or the corresponding force $\mathbf{F} = -\nabla U$ explicitly as a function of only $\mathbf{R}_1, \dots, \mathbf{R}_{I_{\text{max}}}$. [63]

The only complication is that no simple analytic function is known which would express this relation exactly. Even when approximating it as such an analytic function, it will rely on numeric parameters which are not known a priori and need to be fitted to reference data. Despite these limitations and requirements, numerous implementations of such classical interatomic potentials or force fields (FF) exist. [57, 63]

When dealing with covalent compounds, a distinction needs to be made between bonded and non-bonded interactions. Commonly, the potential energy is decomposed into two-, three- and four-body terms. This is illustrated here for the all atom version of the optimized potentials for liquid simulations (OPLS-AA)[14] FF which we used for the organic molecules in ref. [A2]:

- Pair-wise spring potential between covalently bonded atoms

$$U_{\text{bond}} = \sum_i^{\text{bonds}} k_{\text{b},i} (r_i - r_{0,i}) \quad (2.65)$$

with constant $k_{b,i}$ and distance offset $r_{0,i}$ depending on the species (see below) of the bonded atoms and r_i being the distance between them

- ‘Angle bending’ of two neighboring covalent bonds (‘neighboring’ meaning that there is one central atom bonded to at least two other atoms)

$$U_{\text{bend}} = \sum_i^{\text{angles}} k_{\vartheta,i} (\vartheta_i - \vartheta_{0,i}) \quad (2.66)$$

with bond angle ϑ_i and parameters $k_{\vartheta,i}$ and $\vartheta_{0,i}$ in analogy to the bond term

- Torsion in chains of three covalent bonds

$$U_{\text{torsion}} = \sum_i^{\text{torsion angles}} \{V_{1,i}(1 + \cos \varphi_i)/2 + V_{2,i}(1 - \cos 2\varphi_i)/2 + V_{3,i}(1 + \cos 3\varphi_i)/2\} \quad (2.67)$$

with species dependent expansion coefficients $V_{n,i}$ and φ_i being the torsion angle between the two outer bonds, viewed along the central bond. The same functional form can be used for the out-of-plane bending of three bonds around one central atom.[57]

- Coulomb interactions according to eq. (2.1). The atoms are modelled as point charges representing the nuclear charge as well as the electronic charge distribution. In ref. [A2] we used (1.14*)CM1A charges as generated by the online tool LigParGen[14, 38, 41] for organic molecules. The reader is referred to the cited publications for details on this charge model.
- Pair-wise non-bonded interactions in Lennard-Jones form

$$U_{\text{LJ}} = \sum_{i < j}^{\text{atoms}} 4\varepsilon_{ij} [(\sigma_{ij}/r_{ij})^{12} - (\sigma_{ij}/r_{ij})^6] \quad (2.68)$$

with distance r_{ij} between atoms i, j and species dependent parameters ε_{ij} and σ_{ij}

The last two terms (Coulomb and Lennard-Jones) are *not* calculated for atoms pairs which are directly linked by one covalent bond or indirectly by two neighboring bonds. For atoms linked via three covalent bonds, these terms are calculated but halved. For all pairs of atoms which are linked via more than three bonds or not linked at all, they are fully applied.

Many FF models follow this basic scheme, although the functional forms of the individual terms may vary and more detailed terms may be added. Typically, each individual term in the sums needs to be specified by the user, meaning that no bond breaking or forming reactions can be simulated with these basic FFs. Furthermore, the properties of each individual atom depend on its immediate environment. To account for this, each atom is typically assigned a ‘species’ which, in addition to its own nuclear charge, also depends on its bond environment. For example, an alkylic C atom may be assigned a different species than a carboxylic C atom.[57, 63]

Regardless of the specifics discussed so far, ultimately the numeric parameters occurring in the potential energy terms need to be determined. This is typically done by choosing values which reproduce some reference data as exactly as possible. This data can be either measured experimentally or computed on an electronic structure level of theory.[13, 14]

2.5.2 Molecular dynamics, thermostats

This section is adapted from refs. [57, 64].

Once the potential energy function $U(\mathbf{R}_1, \dots, \mathbf{R}_{I_{\max}})$ and some initial positions \mathbf{R}_I and momenta \mathbf{p}_I of the nuclei are chosen, their time development in the NVE ensemble is uniquely defined.⁶ It is, however, not possible to solve the equations of motion analytically except for the simplest systems. In molecular dynamics (MD) simulations, positions and momenta are therefore propagated step-wise in time.

The conceptually simplest implementation of this idea is Euler's method. Choosing a constant time step size Δt , positions and momenta at a time step $t + \Delta t$ are calculated from the values at the previous time step t .

$$\mathbf{R}_I(t + \Delta t) = \mathbf{R}_I(t) + \frac{\mathbf{p}_I(t)}{m_I} \Delta t \quad (2.69a)$$

$$\mathbf{p}_I(t + \Delta t) = \mathbf{p}_I(t) + \mathbf{F}_I(t) \Delta t \quad (2.69b)$$

The atomic force $\mathbf{F}_I = -\nabla_I U$ is the negative gradient of U with respect to \mathbf{R}_I , which is computed straightforwardly when using analytical functions for $U(\mathbf{R}_1, \dots, \mathbf{R}_{I_{\max}})$, such as the FFs discussed in the previous section.

While Euler's method illustrates the general idea well due to its simplicity, it is not commonly used in practice because the approximation of finite time steps introduces an error which accumulates over time. While this is true for any numeric solution to the equations of motion, so-called symplectic algorithms, like velocity-Verlet, are in a sense more stable, as they do (among other things) conserve volumes in phase space over time. One implication is that paths through phase space do not diverge and are uniquely defined by their initial conditions, even after long times. Velocity-Verlet is the default option of the LAMMPS[43, 65] molecular dynamics software which we used in ref. [A2].

$$\mathbf{R}_I(t + \Delta t) = \mathbf{R}_I(t) + \mathbf{v}_I(t) \Delta t + \frac{\mathbf{F}_I(t)}{2m_I} \Delta t^2 \quad (2.70a)$$

$$\mathbf{v}_I(t + \Delta t) = \mathbf{v}_I(t) + \frac{\mathbf{F}_I(t) + \mathbf{F}_I(t + \Delta t)}{2m_I} \Delta t \quad (2.70b)$$

Here, the convention was used of expressing the algorithm in terms of velocities $\mathbf{v}_I = \mathbf{p}_I/m_I$. The entirely equivalent expression in terms of momenta can be derived straightforwardly. Without giving the detailed derivation here, the only differences to Euler's method are the inclusion of a second order term in the expansion of \mathbf{R}_I and the evaluation of velocities from an average force from the current and previous time step.

Regardless of robustness of the used algorithms, the NVE ensemble often represents experimental setups to which results could be compared poorly. More commonly, experimental setups can be approximated as NVT or NpT ensembles. This leads to the challenge of running MD simulations at constant T rather than constant E . Once again referring the reader to the extensive literature for a detailed derivation,[56] a kinetic temperature can be defined via the nuclear kinetic

⁶This is true regardless of whether U is calculated using classical FFs as discussed in the previous section, DFT, or any other model that yields U as a continuously differentiable function of the nuclear coordinates, approximating the nuclei as classical point-like particles.

energy as

$$T = \frac{1}{n_{\text{DOF}}k_{\text{B}}} \sum_I \frac{\|\mathbf{p}_I\|^2}{m_I} \quad (2.71)$$

where n_{DOF} is the number of unconstrained DOF. In the absence of additional constraints, it is simply $3I_{\text{max}} - 6$ where I_{max} is the number of nuclei in the system and the offset of 6 originates from constraining the translation and rotation of the system as a whole to zero.⁷

One might be tempted to enforce eq. (2.71) simply by defining some rule which chooses \mathbf{p}_I accordingly at each time step, e.g. by scaling all velocities by a factor. However, unlike E in the NVE ensemble, which is inherently conserved, T in the NVT ensemble is the result of interaction with a heat bath of constant T . The kinetic temperature according to eq. (2.71) will thus fluctuate even in the NVT ensemble.

To account for this, the Nosé-Hoover thermostat does not enforce the kinetic temperature explicitly. Instead, it simulates the heat bath as an additional DOF. After some derivation, this DOF actually vanishes, instead leading to a ‘friction coefficient’ ξ which acts on the momenta.

$$\frac{d}{dt}\mathbf{R}_I = \frac{\mathbf{p}_I}{m_I} \quad (2.72a)$$

$$\frac{d}{dt}\mathbf{p}_I = \mathbf{F}_I(t) - \xi\mathbf{p}_I \quad (2.72b)$$

Calling ξ a friction coefficient is actually somewhat misleading, as it can become negative if the kinetic temperature is lower than the target value. It changes over time according to

$$\frac{d}{dt}\xi = \left(\sum_I \frac{\|\mathbf{p}_I\|^2}{m_I} - n_{\text{DOF}}k_{\text{B}}T \right) / Q \quad (2.73)$$

effectively comparing the actual kinetic energy to the one expected according to eq. (2.71) and changing ξ accordingly. Q is a free parameter and originally enters the formalism as the virtual mass of the DOF representing the heat bath. It effectively dampens the adaptation of ξ .

2.5.3 Simulating surfaces

This section is adapted from refs. [66–68].

When we want to simulate chemistry at a surface, we are faced with a practical problem. The surface typically extends to meso- or macroscopic scales. The same can be said about the bulk material below the surface. Interactions between atoms are present everywhere, and there is no reasonable point where the simulated system could be truncated. Simulating macroscopic amounts of condensed matter in atomistic detail is computationally intractable, even when using classical FFs.

A common solution to this issue are so-called slab calculations. The normal vector of the surface is defined to be aligned with the z coordinate. Only a finite, typically rectangular, cutout from the surface is simulated. However, instead of truncating the surface at the edge of the cutout, so-called periodic boundary conditions (PBC) are applied in x and y direction. This means that

⁷In the case of linear molecules, it is $3I_{\text{max}} - 5$ instead, because only two rotations can be observed.

formally, the cutout is repeated indefinitely in x and y direction, simulating an infinitely extending surface. Each of these repeated cutouts is identical by construction, so only one of them needs to be simulated. An atom moving through the left ($-x$) edge of the cutout will immediately re-enter it at the right ($+x$) edge, and in y direction accordingly. Similarly, atoms at one edge interact with (the periodic images of) those at the opposite edge.

In z direction, only a finite slab of the material or fluid in question is simulated. This means that effectively, two opposite surfaces are being simulated, one with its normal vector pointing in $+z$ direction, and the other in $-z$ direction. Between these two surfaces, enough material / fluid is placed that it can be reasonably assumed that in the center of the slab its bulk properties are reached. Figure 2.2 shows a water surface covered with a sodium octanoate surfactant modelled in this way, viewed along the upper surface of the slab. Similar simulations were used in ref. [A2].

Evaluation of short ranged FF terms under PBC is not much different from non-periodic systems. Electrostatic interactions, however, are long ranged and the potential generated by all of the infinite repetitions of charges in the system needs to be accounted for. For PBC in all three dimensions, the Ewald summation technique decomposes these interactions into a short ranged part, which can be computed as usual, and a long ranged part which can be computed by Fourier transformation. This method can be adapted for application to slab calculations by separating the slabs far enough from their periodic images and correcting for the interaction between them.

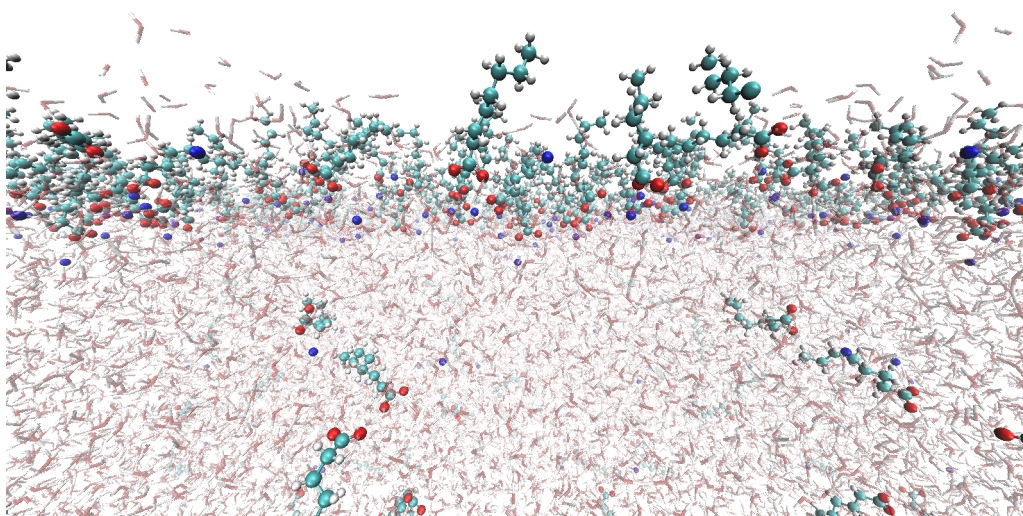


Fig. 2.2: Water surface with a sodium octanoate surfactant, simulated in a slab calculation. Periodic boundary conditions in x and y direction can be seen particularly clearly (keeping perspective in mind) in the octanoate ions in the bulk. Similar calculations were used in ref. [A2], where technical details are elaborated. The advantages of an explicit solvation model are illustrated here in the solute molecules located primarily at the surface, but to a lesser degree also in the bulk. Capturing both behaviours in the same model would be much more challenging for implicit methods.

2.6 Experimental methods

2.6.1 Photoelectron spectroscopy

Let us finally briefly outline the experimental techniques used in ref. [A2]. Section 2.6.1 is adapted from ref. [69] unless indicated otherwise.

The fundamental concept behind photoelectron spectroscopy (PES) is very simple. When illuminating a surface or a gas with light of appropriate angular frequency ω , photons can interact with electrons. The photon is absorbed and its energy, cf. eq. (2.15), is transferred to the electron as kinetic energy. If the electron reaches sufficiently high kinetic energy this way, it may escape the sample. Its kinetic energy can then be measured. However, when working with condensed matter, electrons emitted from the bulk will collide with atoms, preventing them from reaching the detector. PES is thus a surface sensitive method.

The kinetic energy of emitted electrons is given by

$$E_{\text{kin}} = \hbar\omega - \phi - |E_{\text{B}}| \quad (2.74)$$

For surfaces, the work function ϕ is the energy necessary to move one electron from inside the material to vacuum. For gases, this term vanishes. The binding energy E_{B} is the energy necessary to remove one electron from the electronic structure of an atom, molecule or solid. It is the difference between the energies of the system immediately before and immediately after the photon has been absorbed. Since the electronic Hamiltonian has discrete eigenvalues, cf. eq. (2.18), E_{B} will also have discrete values in the case of atoms and molecules. What has been neglected here is that some of the photon energy may be transferred to nuclear motion. These energies are, however, typically small and need not be discussed further for our purposes.

E_{kin} can be measured in various ways. ω is a known property of the used light source. ϕ depends only on the character of the surface.[70] It may be known, and even if it is not, it can be treated as a constant. E_{B} can thus be calculated, either absolute if ϕ is known, or different E_{B} relative to each other if ϕ is not known.[A2] Since the possible initial and final states of the system depend on its composition and structure, valuable information can be obtained from the spectrum of E_{B} . When using light in the X-ray range, core electrons will be emitted. These electrons are initially localized near a nucleus. Their $|E_{\text{B}}|$ depend mostly on the charge of this nucleus and are higher than those of valence electrons, which are more delocalized between nuclei. The chemical environment does, however, give rise to a small but measurable chemical shift, allowing us to distinguish between chemically different cores of the same element based on their binding energies.

2.6.2 Photoelectron angular distributions

When using linearly polarized light in core level PES, i.e. light the photons of which all have the same oscillation direction \mathbf{E}_0 in eq. (2.13), then one would expect electrons to be accelerated and consequently emitted in that same direction. However, as already mentioned above, electrons emitted from below the surface have a chance of colliding with atoms on their way towards the surface. If these collisions are elastic, i.e. if only the propagation directions of the electrons are changed, but not their kinetic energies, then they may still be uniquely identified by E_{B} . They will, however, be detected at different angles than expected.

To be more precise, already if no such collisions occur not all electrons are emitted in the same direction. Rather than that, there is a distribution of emission angles. This photoelectron angular distribution (PAD) can be described by

$$f(\theta) = \frac{1}{4\pi} \left(1 + \frac{\beta}{2} (3 \cos^2(\theta) - 1) \right) \quad (2.75)$$

where θ is the emission angle relative to the polarization direction, and β is the so-called anisotropy parameter. In the absence of any scattering, it is expected to be 2. Higher probability of scattering lowers β . At $\beta = 0$, the emission is completely isotropic, with all angles being equally probable. Since a longer path through the condensed phase corresponds to a higher collision change, β will generally be lower for electrons emitted from deeper beneath the surface.[71]

By measuring the emission intensity in dependence of θ and comparing to eq. (2.75), β can be fitted. In ref. [A2] we use the example for an octanoic acid surfactant on a water surface to show that β obtained this way—after minor corrections, which we elaborate—can be used to characterize the positions of individual atoms relative to the surface. Our results are fully supported by complementary MD simulations using the methods outlined in section 2.5.

Alternatively to PADs, the signal intensities at a single angle also depend on the amount of elastic scattering which the photoelectrons have experienced. Accordingly, they have been used to characterize atomic positions relative to a surface, too.[44] Intensities are, however, influenced by additional effects which do not affect PADs. The latter thus provide a more specific measure of elastic scattering.[A2, 72]

DRAFT

3 Publications

As this dissertation is publication based, a summary of the associated publications is given in this chapter, along with an overview of the individual contributions of myself and my coauthors.

DRAFT

3.1 Piecewise Multipole-Expansion Implicit Solvation for Arbitrarily Shaped Molecular Solutes

Jakob Filser, Karsten Reuter, and Harald Oberhofer

J. Chem. Theory Comput. 2022, 18, 461-478.

DOI: 10.1021/acs.jctc.1c00834

3.1.1 Content

The necessity for a generalization of the MPE method by Sinstein *et al.*[25] for arbitrary solute shapes became clear in the development of an extension of the model which would simulate liquid-gas and liquid-liquid interfaces. The latter idea was already mentioned in Markus Sinstein's dissertation.[45] The basic formalism for the extension of the MPE method to three dielectric regions was developed there and the formal framework as well as some core functionality was already implemented in FHI-aims in this context.

As already described, it became clear that the single multipole series representing the dielectric response in the original version of the method is not guaranteed to converge for molecules larger than ≈ 10 non-hydrogen atoms. Prioritizing robustness over number of features, this issue was addressed first. Our modified method uses an atom-centered piecewise multipole expansion. The method is implemented for serial or parallel execution in the FHI-aims[40] DFT program.

We demonstrate that using expansions up to order $l = 8$, this ensures convergence for a wide range of test systems. Agreement with experimental reference data[39] is shown and improved transferability compared to the previous version of the method is discussed. Lastly, it is demonstrated that in the context of FHI-aims, the method is not a computational bottleneck in the investigated range of molecular sizes. Furthermore, we show that it is faster than the self-consistent continuum solvation (SCCS) model implemented in the Environ package.[18]

In this context, we also made some other, minor improvements to the method, specifically:

- adapting the choice of density ρ used to define the isodensity cavity according to eq. (2.54); as has been shown before,[45] using a superposition of atomic electron densities rather than the instantaneous molecular electron density improves agreement with experiment for anionic solutes
- sampling the cavity boundary more evenly
- imposing the constraint of charge conservation on the long range potential
- developing a sparse iterative solver[73] reducing the memory requirement of our new method
- simplification of the model for $\Delta G_{\text{solv}}^{\text{non-elstat}}$
- investigating the impact of the density functional on the agreement with experimental reference data
- reevaluating the multipole basis for Φ_Q for which we concluded that expansion centers \mathbf{r}_J on the solute's hydrogen atoms can be omitted, saving computational resources.

3.1.2 Individual contributions

The idea to solve the electrostatic problem inside the solvation cavity piecewise and the application of Sinstein's formalism for multiple regions to this idea, including necessary further generalizations, was developed and implemented in FHI-aims by myself, with input from Harald Oberhofer and Karsten Reuter. The same applies to the minor improvements listed above as well as all benchmark and parameterization calculations associated with this publication. The final manuscript was jointly written by Harald Oberhofer, Karsten Reuter and myself.

DRAFT

3.2 Photoelectron angular distributions as sensitive probes of surfactant layer structure at the liquid–vapor interface

Rémi Dupuy, Jakob Filser, Clemens Richter, Robert Seidel, Florian Trinter, Tillmann Buttersack, Christophe Nicolas, John Bozek, Uwe Hergenroth, Harald Oberhofer, Bernd Winter, Karsten Reuter and Hendrik Bluhm

Phys. Chem. Chem. Phys., 2022, 24, 4796–4808.

DOI: 10.1039/d1cp05621b

3.2.1 Content

In an effort to explore the capabilities of PADs as a measure for atomic positions relative to a liquid surface, Rémi Dupuy and coworkers measured PADs of octanoic acid on a water surface (liquid jet) at different concentrations and pH values.

The signals of core electrons emitted from C atoms in the alkylic chain, in the COOH group and in the COO[−] group can be clearly distinguished by the chemical shift in their binding energies. Separate anisotropy parameters β can thus be determined for them. It was found that β was consistently smaller for carboxylic than for alkylic C atoms, implying more elastic scattering and thus an average position deeper towards bulk water. For COO[−], it is smaller than for COOH, both when they are present simultaneously (intermediate pH) and when comparing low and high pH measurements. The difference between alkylic and carboxylic C is thus more pronounced at high pH. Furthermore, all β consistently increase with surfactant concentration. These findings imply that the carboxylic group is consistently oriented towards the aqueous phase, and the alkyl chains towards the gas phase. At high pH, this orientation is more pronounced than at low pH.

We verified this interpretation by MD simulations in the low and high pH limits and at different coverages. Classical MD is perfectly suited for this purpose, as it gives direct access to the property that is indirectly probed in the experiment, i.e. the structure of the surfactant layer. All simulations were performed with the LAMMPS package[43, 65], using a combination of state-of-the-art classical FFs.[13, 14, 38, 41, 42] A periodic water surface in the *NVT* ensemble was simulated to mimick the experimental conditions.

Our MD results provide some mechanistic insight, implying that the orientation of octanoate anions is driven by electrostatic effects, as one would expect, whereas the overall less pronounced vertical orientation of protonated octanoic acid is partially a result of steric crowding, especially at high coverage. All in all, they fully confirm the interpretation of the experimental results brought forward by Rémi Dupuy and coworkers, contributing to this advancement of the PAD methodology.

3.2.2 Individual contributions

Rémi Dupuy and I contributed equally to this work. For the sake of simplicity, the corresponding section of the publication itself is quoted here. The authors are identified by their respective initials.

“ RD and JF wrote the manuscript with inputs from all authors. RD analyzed and interpreted the experimental data with input from HB, BW, and UH. JF performed the MD simulations and interpreted the results with input from HO and KR. RS, CN, and JB provided the beamline endstations and user support for the experiments. HB, BW, and RD conceived the experimental

plans. RD, CR, FT, TB, CN, UH, BW, and HB participated in the beamtimes where the data were acquired. ”[A2]

DRAFT

4 Summary, Conclusions and Outlook

Simulating chemistry in solution and at liquid surfaces or interfaces remains one of the central challenges in computational chemistry. Several established methods already exist which allow us to perform this task, gaining valuable insight. Nonetheless, further improvement is clearly possible in terms of efficiency, accuracy and functionality.

In this work, two related projects in this field were conducted and published. The first[A1] improved the accuracy and transferability of the computationally efficient, yet currently rarely used MPE implicit solvation model. To improve practical applicability, further work will be done in the near future, primarily derivation and implementation of atomic forces in solution. Additionally, sparsification of the multipole basis for the potential Φ_Q outside the solvation cavity may be addressed in the further course, which would allow for applications to very large systems.

In the second project,[A2] classical MD simulations were used to confirm recent advancements in experimental methodology, namely the use of PADs as probes for surfactant structures at a liquid surface. One current limitation lies in the fact that in the used octanoic acid surfactant, PADs could only be distinguished between alkylic and carboxylic C atoms, but not between the different C atoms in the alkylic chain. In a next step, our experimental coworkers and ourselves will apply the same methods to different surfactants which allow for a finer resolution in that sense. Finer resolution on the computational side can be achieved by computing atomic positions relative to an instantaneous water surface.[74]

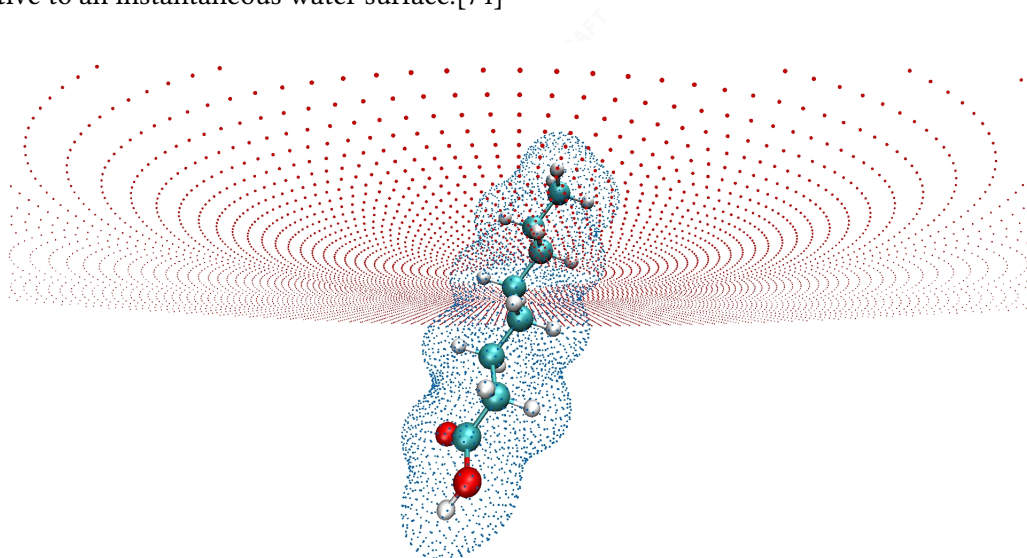


Fig. 4.1: Octanoic acid molecule with discretized cavity surface and liquid surface towards vacuum or another liquid. Interfaces between cavity subregions not shown for reasons of clarity.

Although the two projects may appear to be thematically disjoint at first glance, a connection will be established once the implementation of the extended MPE method for interfaces is finalized

and tested. Direct comparison to results both from experiment and classical MD simulations, and evaluation of the advantages and shortcomings of both methods will then be possible. Our MD simulations demonstrate that the sensitivity of solvation at liquid surfaces to influences such as coverage and protonation state can be appropriately described by atomistic models. Since these effects emerge from interactions on an atomic scale, attempting to correctly reproduce them in a coarse grained model is a challenging and interesting task. Mentionable work in this direction has already been done in the context of this dissertation, and comprehensive testing is subject to ongoing work. Figure 4.1 shows how the interface discretization carried out in an MPE calculation looks like for an octanoic acid molecule. The cavity surface and the liquid surface can be treated in the exact same way, as already described and largely implemented by Markus Sinstein in his dissertation.[45] The same can be said about the boundaries between the cavity subregions in our modified MPE method, facilitating the combination of the two methods and allowing for an accurate solution of the electrostatic problem at a dielectric interface.

DRAFT

Acknowledgements

I want to thank Harald Oberhofer and Karsten Reuter for their supervision, helpful advice, the great opportunities they provided and their constant support. Apart from these things that helped me as an individual, the many fantastic group activities shall not be left unmentioned. I will keep fond memories of the DPG conferences we went to as a whole group, the food nights, christmas parties, and of course our legendary group retreats. I also thank the various people who planned the latter over the course of time.

Obviously, these team events would not have been any fun if it weren't for our wonderful group members. I want to thank all of you, not only for the fun, but just as much for the inspiring scientific discussions we had. First and foremost, Markus Sinstein shall be mentioned here, who was my predecessor working on the MPE model. His guidance made my start into the project as smooth as I could imagine. On a similar notion, I would have been completely lost on classical force fields methods without the aid of David Egger. Big thanks to both of you for being awesome colleagues!

I also want to thank the many people who helped me with the small, day-to-day issues, like our first level support team, the people with whom I did the tutorials, the FHI-aims developers team, and of course Ruth Mösch. Thanks to her, I was able to live happily without having to worry about the trials and tribulations of administration for my entire time as a PhD student.

I especially thank my parents who always supported me personally and emotionally¹, regardless of whether or not we agreed on any particular issue. Without you, I would not be here, and I certainly would not be the person I am. Last but not least, I thank my wonderful girlfriend Malena, who I had the great luck to have by my side for the second half of my PhD time. Everything is just better when you are around :-)

Munich, April 2022

¹and financially

Bibliography

- [A1] J. Filser, K. Reuter, and H. Oberhofer, *Journal of Chemical Theory and Computation* **18**, PMID: 34935366, 461 (2022) (cit. on pp. 2, 7, 19–23, 37).
- [A2] R. Dupuy, J. Filser, C. Richter, R. Seidel, F. Trinter, T. Buttersack, C. Nicolas, J. Bozek, U. Hergenbahn, H. Oberhofer, B. Winter, K. Reuter, and H. Bluhm, *Phys. Chem. Chem. Phys.* **24**, 4796 (2022) (cit. on pp. 3, 23–25, 27–29, 36, 37).
- [1] Y. Levy and J. N. Onuchic, *Annu. Rev. Biophys. Biomol. Struct.* **35**, 389 (2006) (cit. on p. 1).
- [2] S. Kalepu and V. Nekkanti, *Acta Pharm. Sin. B* **5**, 442 (2015) (cit. on p. 1).
- [3] J. J. Varghese and S. H. Mushrif, *React. Chem. Eng.* **4**, 165 (2019) (cit. on pp. 1, 2).
- [4] X.-B. Cheng, C.-Z. Zhao, Y.-X. Yao, H. Liu, and Q. Zhang, *Chem* **5**, 74 (2019) (cit. on p. 1).
- [5] G. Fang, J. Zhou, A. Pan, and S. Liang, *ACS Energy Lett.* **3**, 2480 (2018) (cit. on p. 1).
- [6] S. Anantharaj, S. R. Ede, K. Sakthikumar, K. Karthick, S. Mishra, and S. Kundu, *ACS Catal.* **6**, 8069 (2016) (cit. on p. 1).
- [7] O. Andreussi and G. Fisicaro, *Int. J. Quantum Chem.* **119**, e25725 (2019) (cit. on pp. 1, 2).
- [8] J. Tomasi, B. Mennucci, and R. Cammi, *Chem. Rev.* **105**, 2999 (2005) (cit. on pp. 1, 2, 6, 7, 16–19).
- [9] K. Schwarz and R. Sundararaman, *Surf. Sci. Rep.* **75**, 100492 (2020) (cit. on pp. 1, 2).
- [10] S. Ringe, N. G. Hörmann, H. Oberhofer, and K. Reuter, *Chemical Reviews* **0**, PMID: 34928131, null (0) (cit. on pp. 1, 2, 7, 16–18, 22).
- [11] H. J. C. Berendsen, J. P. M. Postma, W. F. van Gunsteren, and J. Hermans, “Interaction models for water in relation to protein hydration,” in *Intermolecular forces: proceedings of the fourteenth jerusalem symposium on quantum chemistry and biochemistry held in jerusalem, israel, april 13–16, 1981*, edited by B. Pullman (Springer Netherlands, 1981), pp. 331–342 (cit. on pp. 1, 2).
- [12] H. J. C. Berendsen, J. R. Grigera, and T. P. Straatsma, *J. Phys. Chem.* **91**, 6269 (1987) (cit. on pp. 1, 2).
- [13] Y. Wu, H. L. Tepper, and G. A. Voth, *J. Chem. Phys.* **124**, 024503 (2006) (cit. on pp. 1, 2, 24, 35).
- [14] W. L. Jorgensen, J. Tirado-Rives, and B. J. Berne, *Proc. Natl. Acad. Sci. U. S. A.* **102**, 6665 (2005) (cit. on pp. 2, 23, 24, 35).
- [15] P. S. Gil and D. J. Lacks, *J. Chem. Phys.* **145**, 204705 (2016) (cit. on p. 2).
- [16] A. F. de Moura, K. Bernardino, O. V. de Oliveira, and L. C. G. Freitas, *J. Phys. Chem. B* **115**, PMID: 22026457, 14582 (2011) (cit. on p. 2).

- [17] D. A. Scherlis, J.-L. Fattebert, F. Gygi, M. Cococcioni, and N. Marzari, *J. Chem. Phys.* **124**, 074103 (2006) (cit. on pp. 2, 22).
- [18] O. Andreussi, I. Dabo, and N. Marzari, *J. Chem. Phys.* **136**, 064102 (2012) (cit. on pp. 2, 18, 19, 22, 23, 33).
- [19] A. V. Marenich, C. J. Cramer, and D. G. Truhlar, *J. Phys. Chem. B* **113**, 6378 (2009) (cit. on pp. 2, 16, 17, 19, 22).
- [20] G. Fiscaro, L. Genovese, O. Andreussi, S. Mandal, N. N. Nair, N. Marzari, and S. Goedecker, *J. Chem. Theory Comput.* **13**, 3829 (2017) (cit. on pp. 2, 19).
- [21] O. Andreussi, N. G. Hörmann, F. Nattino, G. Fiscaro, S. Goedecker, and N. Marzari, *J. Chem. Theory Comput.* **15**, 1996 (2019) (cit. on pp. 2, 19).
- [22] S. Ringe, H. Oberhofer, C. Hille, S. Matera, and K. Reuter, *J. Chem. Theory Comput.* **12**, 4052 (2016) (cit. on pp. 2, 19).
- [23] A. Klamt and G. Schüürmann, *J. Chem. Soc. Perkin Trans. 2*, 799 (1993) (cit. on pp. 2, 19, 21).
- [24] C. P. Kelly, C. J. Cramer, and D. G. Truhlar, *J. Chem. Theory Comput.* **1**, 1133 (2005) (cit. on pp. 2, 19).
- [25] M. Sinstein, C. Scheurer, S. Matera, V. Blum, K. Reuter, and H. Oberhofer, *J. Chem. Theory Comput.* **13**, 5582 (2017) (cit. on pp. 2, 12, 18–23, 33).
- [26] F. Lipparini, B. Stamm, E. Cancès, Y. Maday, and B. Mennucci, *J. Chem. Theory Comput.* **9**, 3637 (2013) (cit. on pp. 2, 21).
- [27] E. Cancès, Y. Maday, and B. Stamm, *J. Chem. Phys.* **139**, 054111 (2013) (cit. on pp. 2, 21).
- [28] M. Nottoli, R. Nifosì, B. Mennucci, and F. Lipparini, *J. Chem. Theory Comput.* **17**, 5661 (2021) (cit. on pp. 2, 21).
- [29] K. Mathew, R. Sundararaman, K. Letchworth-Weaver, T. A. Arias, and R. G. Hennig, *J. Chem. Phys.* **140**, 084106 (2014) (cit. on p. 2).
- [30] J. G. Kirkwood, *J. Chem. Phys.* **2**, 351 (1934) (cit. on pp. 2, 20).
- [31] L. Onsager, *J. Am. Chem. Soc.* **58**, 1486 (1936) (cit. on pp. 2, 19, 20).
- [32] J.-L. Rivail and D. Rinaldi, *Chem. Phys.* **18**, 233 (1976) (cit. on pp. 2, 19, 20).
- [33] D. Rinaldi, M. F. Ruiz-Lopez, and J.-L. Rivail, *J. Chem. Phys.* **78**, 834 (1983) (cit. on p. 2).
- [34] V. Dillet, D. Rinaldi, J. G. Ángyán, and J.-L. Rivail, *Chem. Phys. Lett.* **202**, 18 (1993) (cit. on pp. 2, 19, 20).
- [35] D. Rinaldi, A. Bouchy, J.-L. Rivail, and V. Dillet, *J. Chem. Phys.* **120**, 2343 (2004) (cit. on pp. 2, 20).
- [36] J.-L. Fattebert and F. Gygi, *Journal of Computational Chemistry* **23**, 662 (2002) (cit. on pp. 2, 7).
- [37] C. Amovilli and B. Mennucci, *J. Phys. Chem. B* **101**, 1051 (1997) (cit. on p. 2).
- [38] L. S. Dodda, J. Z. Vilseck, J. Tirado-Rives, and W. L. Jorgensen, *J. Phys. Chem. B* **121**, 3864 (2017) (cit. on pp. 2, 24, 35).

- [39] A. V. Marenich, C. P. Kelly, J. D. Thompson, G. D. Hawkins, C. C. Chambers, D. J. Giesen, P. Winget, C. J. Cramer, and D. G. Truhlar, *Minnesota Solvation Database, version 2012*, University of Minnesota (Minneapolis, 2012) (cit. on pp. 2, 22, 33).
- [40] V. Blum, R. Gehrke, F. Hanke, P. Havu, V. Havu, X. Ren, K. Reuter, and M. Scheffler, *Comput. Phys. Commun.* **180**, 2175 (2009) (cit. on pp. 2, 8, 10, 19, 33).
- [41] L. S. Dodda, I. Cabeza de Vaca, J. Tirado-Rives, and W. L. Jorgensen, *Nucleic Acids Res.* **45**, W331 (2017) (cit. on pp. 2, 24, 35).
- [42] M. M. Reif and P. H. Hünenberger, *J. Chem. Phys.* **134**, 144104 (2011) (cit. on pp. 3, 35).
- [43] S. Plimpton, A. Kohlmeyer, A. Thompson, S. Moore, and R. Berger, *LAMMPS, version 24 Dec 2020*, (2020) (cit. on pp. 3, 25, 35).
- [44] M.-M. Walz, J. Werner, V. Ekholm, N. L. Prisle, G. Öhrwall, and O. Björneholm, *en, Phys. Chem. Chem. Phys.* **18**, 6648 (2016) (cit. on pp. 3, 29).
- [45] M. Sinstein, “*Multipole Expansion Implicit Solvation Model in Full Potential DFT*” Dissertation (Technische Universität München, 2018) (cit. on pp. 3, 6, 10, 18, 33, 38).
- [46] R. Bonaccorsi, M. Hodošček, and J. Tomasi, *Journal of Molecular Structure: THEOCHEM* **164**, 105 (1988) (cit. on p. 3).
- [47] R. Bonaccorsi, F. Floris, P. Palla, and J. Tomasi, *Thermochimica Acta* **162**, 213 (1990) (cit. on p. 3).
- [48] R. Bonaccorsi, E. Ojalvo, P. Palla, and J. Tomasi, *Chemical Physics* **143**, 245 (1990) (cit. on p. 3).
- [49] L. Frediani, C. S. Pomelli, and J. Tomasi, *Phys. Chem. Chem. Phys.* **2**, 4876 (2000) (cit. on p. 3).
- [50] J. D. Jackson, *Classical Electrodynamics*, 3rd ed. (Wiley, 1998) (cit. on pp. 5, 7, 19).
- [51] D. Griffiths, *Introduction to Quantum Mechanics* (Prentice Hall, 1994) (cit. on pp. 7, 8, 14).
- [52] W. Koch and M. C. Holthausen, *A Chemist’s Guide to Density Functional Theory*, 2nd ed. (Wiley - VCH, 2001) (cit. on pp. 7, 10).
- [53] J. Sun, A. Ruzsinszky, and J. P. Perdew, *Phys. Rev. Lett.* **115**, 036402 (2015) (cit. on p. 12).
- [54] W. J. Rankin, *Chemical Thermodynamics: Theory and Applications*, 1st ed. (CRC Press / Taylor & Francis, 2019) (cit. on pp. 14, 16).
- [55] R. Holyst and A. Poniewierski, *Thermodynamics for Chemists, Physicists and Engineers* (Springer, 2012) (cit. on p. 14).
- [56] W. Nolting, *Theoretical Physics 8: Statistical Physics* (Springer, 2018) (cit. on pp. 14, 25).
- [57] C. J. Cramer, *Essentials of Computational Chemistry: Theories and Models*, 2nd ed. (Wiley, 2004) (cit. on pp. 14, 23–25).
- [58] C. P. Kelly, C. J. Cramer, and D. G. Truhlar, *The Journal of Physical Chemistry B* **111**, PMID: 17214493, 408 (2007) (cit. on p. 16).
- [59] C. Hille, S. Ringe, M. Deimel, C. Kunkel, W. E. Acree, K. Reuter, and H. Oberhofer, *J. Chem. Phys.* **150**, 041710 (2019) (cit. on pp. 17, 22).
- [60] R. J. A. Tough and A. J. Stone, *J. Phys. A: Math. Gen.* **10**, 1261 (1977) (cit. on p. 21).

- [61] M. J. Caola, *J. Phys. A: Math. Gen.* **11**, L23 (1978) (cit. on p. 21).
- [62] F. V. Grigor'ev, M. V. Bazilevskii, S. N. Zhabin, A. N. Romanov, and V. B. Sulimov, *Russian Journal of Physical Chemistry A* **82**, 517 (2008) (cit. on p. 22).
- [63] F. Jensen, *Introduction to Computational Chemistry*, 2nd ed. (Wiley, 2004) (cit. on pp. 23, 24).
- [64] D. Frenkel and B. Smit, *Understanding Molecular Simulation: From Algorithms to Applications*, 2nd ed. (Academic Press, 2001) (cit. on p. 25).
- [65] S. Plimpton, *J. Comput. Phys.* **117**, 1 (1995) (cit. on pp. 25, 35).
- [66] M. P. Allen and D. J. Tildesley, *Computer Simulation of Liquids*, 2nd ed. (Oxford, 2017) (cit. on p. 26).
- [67] I.-C. Yeh and M. L. Berkowitz, *The Journal of Chemical Physics* **111**, 3155 (1999) (cit. on p. 26).
- [68] The LAMMPS Developers, *LAMMPS Documentation: <https://docs.lammps.org/Manual.html>*, accessed 19.04.2022, (2022) (cit. on p. 26).
- [69] S. Hüfner, *Photoelectron Spectroscopy: Principles and Applications*, 3rd ed. (Springer, 2003) (cit. on p. 28).
- [70] C. Kittel, *Introduction to Solid State Physics*, 7th ed. (Wiley, 1996) (cit. on p. 28).
- [71] R. Dupuy, C. Richter, B. Winter, G. Meijer, R. Schlögl, and H. Bluhm, *J. Chem. Phys.* **154**, 060901 (2021) (cit. on p. 29).
- [72] T. Lewis, B. Winter, S. Thürmer, R. Seidel, A. B. Stephansen, J. A. Freites, D. J. Tobias, and J. C. Hemminger, *J. Phys. Chem. C* **123**, 8160 (2019) (cit. on p. 29).
- [73] C. C. Paige and M. A. Saunders, *ACM Trans. Math. Softw.* **8**, 43 (1982) (cit. on p. 33).
- [74] Z. Liu, T. Stecher, H. Oberhofer, K. Reuter, and C. Scheurer, *Molecular Physics* **116**, 3409 (2018) (cit. on p. 37).